A thermal plume model for the Martian convective boundary layer

Arnaud Colaïtis, Aymeric Spiga, Frédéric Hourdin, Catherine Rio, François Forget, Ehouarn Millour

▶ **To cite this version:**

Arnaud Colaïtis, Aymeric Spiga, Frédéric Hourdin, Catherine Rio, François Forget, et al.. A thermal plume model for the Martian convective boundary layer. Journal of Geophysical Research. Planets, 2013, 118 (7), pp.1468-1487. 10.1002/jgre.20104 . hal-01089504

HAL Id: hal-01089504
https://hal.science/hal-01089504

Submitted on 3 Dec 2014

HAL is a multi-disciplinary open access archive for the deposit and dissemination of scientific research documents, whether they are published or not. The documents may come from teaching and research institutions in France or abroad, or from public or private research centers.

L'archive ouverte pluridisciplinaire **HAL**, est destinée au dépôt et à la diffusion de documents scientifiques de niveau recherche, publiés ou non, émanant des établissements d'enseignement et de recherche français ou étrangers, des laboratoires publics ou privés.

JOURNAL OF GEOPHYSICAL RESEARCH: PLANETS, VOL. 118, 1468–1487, doi:10.1002/jgre.20104, 2013

A thermal plume model for the Martian convective boundary layer

A. Colaïtis,[1] A. Spiga,[1] F. Hourdin,[1] C. Rio,[1] F. Forget,[1] and E. Millour[1]

Received 31 July 2012; revised 12 June 2013; accepted 17 June 2013; published 25 July 2013.

[1] The Martian planetary boundary layer (PBL) is a crucial component of the Martian climate system. Global climate models (GCMs) and mesoscale models (MMs) lack the resolution to predict PBL mixing which is therefore parameterized. Here we propose to adapt the "thermal plume" model, recently developed for Earth climate modeling, to Martian GCMs, MMs, and single-column models. The aim of this physically based parameterization is to represent the effect of organized turbulent structures (updrafts and downdrafts) on the daytime PBL transport, as it is resolved in large-eddy simulations (LESs). We find that the terrestrial thermal plume model needs to be modified to satisfyingly account for deep turbulent plumes found in the Martian convective PBL. Our Martian thermal plume model qualitatively and quantitatively reproduces the thermal structure of the daytime PBL on Mars: superadiabatic near-surface layer, mixing layer, and overshoot region at PBL top. This model is coupled to surface layer parameterizations taking into account stability and turbulent gustiness to calculate surface-atmosphere fluxes. Those new parameterizations for the surface and mixed layers are validated against near-surface lander measurements. Using a thermal plume model moreover enables a first-order estimation of key turbulent quantities (e.g., PBL height and convective plume velocity) in Martian GCMs and MMs without having to run costly LESs.

Citation: Colaïtis, A., A. Spiga, F. Hourdin, C. Rio, F. Forget, and E. Millour (2013), A thermal plume model for the Martian convective boundary layer, *J. Geophys. Res. Planets*, *118*, 1468–1487, doi:10.1002/jgre.20104.

1. Introduction

[2] The exploration of the Martian environment yields many examples of planetary boundary layer (PBL) phenomena commonly encountered on Earth: convective cloud streets [*Malin and Edgett*, 2001], dust devils (i.e., dusty convective vortices) [see *Balme and Greeley*, 2006, for a review], afternoon growth of the mixing layer [*Hinson et al.*, 2008] associated with turbulent fluctuations of near-surface temperature [*Smith et al.*, 2006], and nighttime stable conditions with low-level jets [*Savijärvi and Siili*, 1993]. The Martian environment can be seen as a large dusty desert in which PBL dynamics is more extreme than on Earth. Owing to the thin CO_2 atmosphere and low thermal inertia of the surface, the Martian PBL is radiatively controlled and undergoes a strong diurnal cycle with temperature gradients in the surface layer following superadiabatic regimes in daytime and ultrastable regimes in nighttime [e.g., *Schofield et al.*, 1997; *Smith et al.*, 2006]. In the afternoon, the mixed layer is sometimes almost as deep as one atmospheric scale height ($\sim$ 10 km) [*Hinson et al.*, 2008] and, in many cases, deeper than the afternoon PBL in most regions on Earth [*Spiga*, 2011]. The Martian daytime PBL is also characterized by the negligible role played by moist processes and, conversely, the crucial role played by the absorption of infrared emission from the surface by CO_2 and, to a lesser extent, dust [*Haberle et al.*, 1993; *Sävijarvi*, 1999].

[3] The existing three-dimensional nonhydrostatic mesoscale models for the Martian atmosphere can be used to assess Martian PBL dynamics in daytime [*Toigo and Richardson*, 2003; *Michaels and Rafkin*, 2004; *Richardson et al.*, 2007; *Tyler et al.*, 2008; *Spiga et al.*, 2010]. In so-called large-eddy simulations (LESs), the grid spacing is lowered to a few tens of meters so as to resolve the largest turbulent eddies, responsible for most of the energy transport within the PBL [*Lilly*, 1962]. LESs have demonstrated that from late morning to sunset, PBL dynamics associated with superadiabatic near-surface temperature gradients comprise powerful narrow updrafts with vertical velocities of 10–20 m s^{-1} and broad downdrafts with vertical velocities of 5–10 m s^{-1}, organized in a polygonal cellular structure [*Michaels and Rafkin*, 2004; *Spiga and Forget*, 2009]. Recent LESs reproduce the regional variability of PBL depth revealed through observations and dominated on Mars by radiative forcing inside the boundary layer [*Spiga et al.*, 2010].

[4] Convective plumes, i.e., the largest eddies resolved in LESs, are named nonlocal turbulence, or organized turbulence: e.g., updrafts entrain air from the surface layer and detrain it at several kilometers above the ground in daytime (cf. Figure 1). Conversely, local turbulence refers to

Additional supporting information may be found in the online version of this article.

[1]Laboratoire de Météorologie Dynamique, Université Pierre et Marie Curie, Institut Pierre Simon Laplace, Centre National de la Recherche Scientifique, Paris, France.

Corresponding author: A. Spiga, Laboratoire de Météorologie Dynamique Tour 45, 3e et., Université P&M Curie, BP99, 4 pl. Jussieu, 75005 Paris, France. (aymeric.spiga@upmc.fr)

©2013. American Geophysical Union. All Rights Reserved.
2169-9097/13/10.1002/jgre.20104

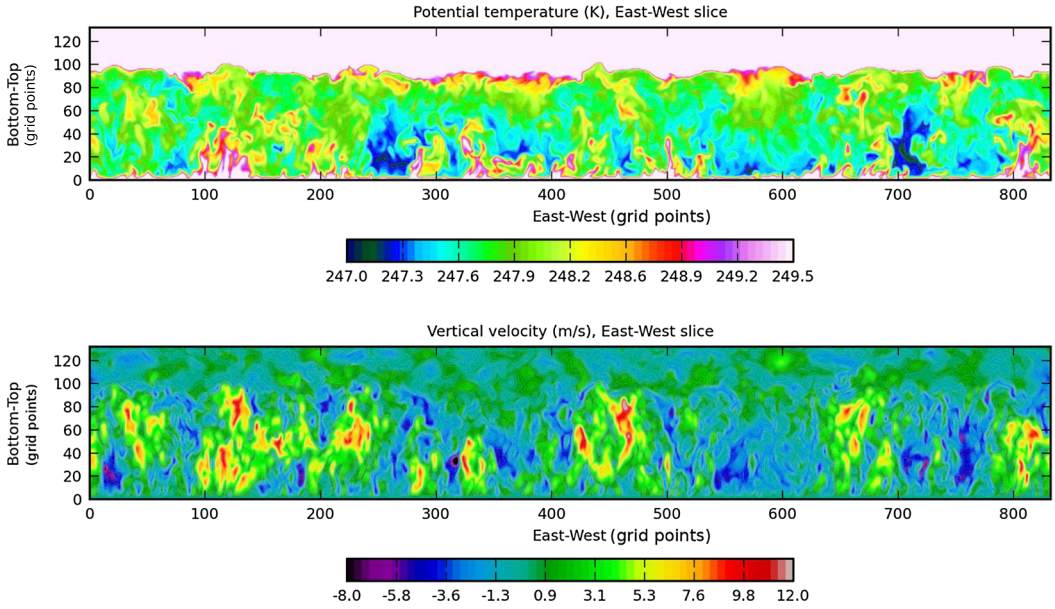

Figure 1. LES results for the Martian convective boundary layer. (top) Slices of potential temperature (K) and (bottom) vertical velocity (m s^{-1}). Results are from simulation C.large, taken at local time 15:00 along the West-East direction (aligned with the background wind). Horizontal resolution for this simulation is 100 m between grid points so that total domain extent is 83 km. Vertical resolution is about 75 m (except in the first few layers where the mesh is refined for the surface layer).

turbulent motions which do not induce vertical transport over a significant fraction of the PBL depth. Both large eddies, resolved by LESs, and small eddies, unresolved by LESs, contribute to local turbulent mixing. In global climate models (GCMs), mesoscale models (MMs), and single-column models (SCMs), all three kinds of turbulent structures in the PBL (nonlocal large eddies, local large eddies, and small-scale eddies) are left unresolved and hence must be parameterized.

[5] Parameterizing PBL vertical transport in GCMs and MMs is a key element to accurately predict the large-scale and regional variability of winds and temperature, volatile mixing, and surface-atmosphere interactions (e.g., dust lifting). Local turbulence is usually parameterized by turbulent closure schemes, where mixing is obtained through local diffusion processes [*Mellor and Yamada*, 1982, for a review]. A remaining crucial issue is how to model nonlocal turbulence, which participates significantly to the total turbulent mixing budget of the daytime convective PBL.

[6] The crudest parameterization for nonlocal turbulence consists in replacing an unstable PBL profile by its neutral equivalent while conserving mass and energy (convective adjustment). This approach strongly underestimates daytime near-surface temperatures in Martian GCMs and MMs [*Rafkin*, 2003; *Spiga and Forget*, 2009] because the radiatively controlled superadiabatic layers in the first hundreds of meters above the Martian surface cannot be reproduced. More sophisticated techniques, inherited from terrestrial modeling, were adopted instead [*Tyler et al.*, 2002; *Richardson et al.*, 2007]. A widely used method in Martian models is to parameterize nonlocal turbulence by adding a countergradient term in local turbulent diffusion schemes [*Troen and Mahrt*, 1986].

[7] "Thermal plume models" have been recently developed in terrestrial GCMs and MMs to parameterize nonlocal large eddies and the resulting transport in the PBL [*Hourdin et al.*, 2002; *Soares et al.*, 2004; *Rio and Hourdin*, 2008]. Their name reflects their aim to model nonlocal transport by describing convective plumes in the daytime PBL more explicitly than countergradient schemes. In other words, thermal plume models attempt to parameterize not only the mixed layer within the PBL but also the transport processes responsible for it. These schemes, also named mass flux PBL schemes, are now routinely used in several terrestrial GCMs [*Teixeira et al.*, 2011; *Hourdin et al.*, 2012] and were shown to yield a better representation of water vapor transport from the surface to the free atmosphere.

[8] Using a thermal plume model in Martian GCMs and MMs has a great potential for improving the representation of PBL processes in these models:

[9] 1. The vigorous daytime PBL mixing on Mars by strong updrafts and downdrafts makes the thermal plume model especially relevant to the Martian environment. Adapting this model to Mars in turn offers the possibility to test it, and possibly improve it, by using it in an extraterrestrial desert, devoid of any significant moist processes, and prone to original and extreme PBL dynamics.

[10] 2. *Tyler et al.* [2008] noticed the daytime PBL depth parameterized in Martian MMs is significantly underestimated compared to LESs. A possible explanation might be that countergradient schemes are not accurate enough to represent nonlocal turbulence in the strongly convective Martian PBL.

[11] 3. Thermal plume models allow for key PBL variables (e.g., updraft/downdraft speeds) to be estimated to first order in GCMs and MMs. Furthermore, a proxy for near-surface gustiness can be obtained from thermal plume

Table 1. Settings of Reference LES for the Design of the Martian Thermal Plume Model[a]

	L_s (Degree)	φ (°N)	λ (°E)	$\mathcal{T}$ (tiu)	$\mathcal{A}$	T_s (K, at 06:00)	h (km)	p_s (P_a, at 6:00)	τ
A	47.1	21.8	205.0	55	0.27	167.32	–3.9	857.0	0.5
C	52.1	12.3	237.2	60	0.30	161.15	+2.5	480.7	0.5
I	47.8	20.6	74.0	300	0.13	192.56	–0.5	629.0	0.5
Z	67.0	–10.2	236.6	42	0.28	153.04	+8.4	265.6	0.5
Exo	244	–1.82	–6.15	238	0.205	197.3	–1.4	717.9	0.5
E	0	0	0	50	0.10	186.26	–1.5	670.0	0.05

[a]L_s is the solar longitude, φ is the north latitude, λ is the east longitude, $\mathcal{T}$ is the surface thermal inertia in J m^{-2} K^{-1} s$^{-1/2}$ (tiu), $\mathcal{A}$ is the surface albedo, T_s is the surface temperature at local time 6:00 (corresponding to starting time for simulations), h is the altitude with respect to the MOLA reference, p_s is the surface pressure at local time 06:00, and τ is the dust opacity ($\tau = 0.5$ corresponds to moderately dusty conditions on Mars). Cases A, C, I, and Z are inspired by *Hinson et al.* [2008] observations and follow their naming convention [see also *Spiga et al*., 2010]. Case Exo (Exomars) is a simulation at Meridiani Planum (reference site for Exomars preparatory studies). Case E is an "extreme" convection case obtained by assuming a clear atmosphere and low thermal inertia and albedo.

models, which permits a more realistic representation of surface-atmosphere fluxes.

[12] Here we report the first adaptation of a thermal plume model to simulate PBL dynamics and mixing in Martian GCMs, MMs, and SCMs. We describe in section 2 the methods used to analyze and sample the convective structures in LES of the Martian daytime PBL. The thermal plume model for Mars is formulated in sections 3 and 4. An improved surface layer model for Mars, coupled to parameterized turbulent gustiness in the thermal plume model, is proposed in section 5. In section 6, we test our new PBL parameterizations, discuss their performances compared to LES results, and validate their predictions with in situ data on Mars. In all sections, symbols are defined at their first appearance in the paper and listed within the supplementary material.

2. Large-Eddy Simulations of Martian Daytime PBL Convection

[13] A prerequisite for the adaptation of the thermal plume model to Mars is a characterization of the nonlocal convective plumes in the Martian daytime PBL. This is done through LES and sampling techniques adapted for Mars.

2.1. Methodology and Results

[14] Martian LESs are carried out with the Laboratoire de Météorologie Dynamique (LMD) Martian Mesoscale Model by *Spiga and Forget* [2009], based on the Weather Research Forecast dynamical core [*Skamarock and Klemp*, 2008] and its adaptations for LES [*Moeng et al.*, 2007]. We adopt similar settings and physical parameterizations as in *Spiga et al.* [2010] (see also *Forget et al.* [1999] and *Madeleine et al.* [2011] for parameterizations used in LMD models, namely, radiative transfer). We use a $101 \times 101 \times 201$ grid with a horizontal resolution of 100 m and a vertical resolution of 75 m. *Spiga et al.* [2010] showed that these LES correctly represent the dynamics of the daytime convective PBL. Finer resolution LESs are performed in this paper for verification purposes and a better sampling of convective structures.

[15] LESs are performed over a large range of environmental conditions relevant to Mars in order to assess the relevance of the thermal plume approach. Those cases, summarized in Tables 1 and 2, are inspired both by reference cases for which observations are available (radio occultations by *Hinson et al.* [2008] compared to LES by *Spiga et al.* [2010]) and extreme cases for PBL convection obtained, e.g., by setting low albedo, thermal inertia, or surface pressure. All simulations are initialized at local time 06:00 (before convection becomes active) using the climatologies of the Martian LMD GCM [*Forget et al.*, 1999] available in the "Mars Climate Database" (MCD) [*Millour et al.*, 2008]. A background wind of 10 m s^{-1} is prescribed to represent typical synoptic/regional circulations on Mars (the indicated value is valid within the mixed layer; in the surface layer, momentum mixing and near-surface friction produce background wind speed lower than prescribed). To improve the

Table 2. Additional Cases Associated With Reference Cases Described in Table 1[a]

	Grid N_x x N_y x N_z	dx = dy (m)	$\Delta x = \Delta y$ (km)	dz (m)	Δz (km)	τ	u (m/s)
default	$101 \times 101 \times 201$	100	10.0	75	15.0	0.5	10.0
.hr	$257 \times 257 \times 301$	50	12.8	50	15.0	-	-
.large	$833 \times 833 \times 133$	100	83.2	75	10	-	-
.t2	-	-	-	-	-	2	-
.w30	-	-	-	-	-	-	30.0

[a]dx and dy (respectively, Δx and Δy) are horizontal resolution (respectively, domain size) in the West-East and South-North directions, u is the background wind in the West-East direction, and dz is the vertical resolution above the surface layer. "-" indicates default value. Changes in settings are mostly applied to cases A and C.

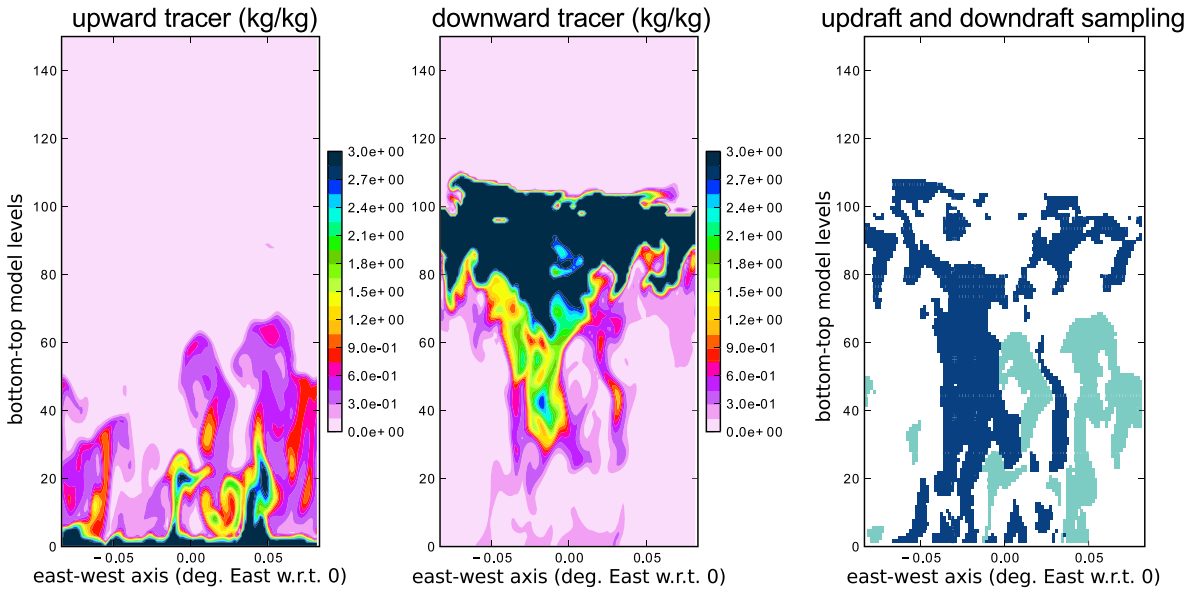

Figure 2. Using LES to sample organized convective structures (case I at local time 15:20). Slices of (left) upward and (middle) downward decaying tracer concentrations (kg kg^{-1}), respectively, emitted at the surface and in the PBL top. (right) Results of the conditional sampling selection where dark blue is downdraft sampling and light green is updraft sampling.

characterization of PBL nonlocal turbulence for the thermal plume model, namely, updraft velocity, entrainment, and detrainment rates, we also ran a more computationally challenging LES over a 80 km × 80 km domain for case C. About 30 updrafts are featured in this LES, compared to 1–2 with reference settings.

[16] Figure 1 illustrates the typical nonlocal large eddies which develop in the Martian convective PBL in daytime in this reference simulation. The observed "flame-like" structures are associated with strong vertical velocities and positive potential temperature anomalies compared to slab averages (by slab we mean a domain-wide square at a given altitude or model level). These correspond to updrafts and exhibit large buoyancies. Cold areas can also be identified, mostly corresponding to areas of negative vertical velocities. Plumes detrain mainly at the top of the boundary layer, depositing the remainder of the advected heat there.

2.2. Sampling Nonlocal Structures

[17] A first step towards parameterizing the nonlocal turbulence resolved by LESs is to sample organized structures, namely, updrafts and downdrafts. Figure 1 emphasizes the difficulty in choosing between what can be considered as part of an updraft and what can be considered as the environment. The distinction between the two must be formulated adequately, as the variations of the mass flux of the plume, hence vertical mixing, are directly connected to entrainment and detrainment rates.

[18] Several criteria have been proposed to sample organized structures in terrestrial LESs, mostly based on quantities related to water. For Mars, we use the tracer-based conditional sampling formulation proposed by *Couvreux et al.* [2010], which is not water based and shows satisfactory results with respect to other methods in Earth LESs. A tracer is emitted in the first layer of the LES model, with a decaying concentration whose half-life is determined by the time it would take a particle to reach the top of the PBL. Typical timescales for this migration on Mars are between 5 and 10 min, which is much less than that on Earth (typically 20 to 60 min). Figure 2 shows the concentration of such a decaying tracer emitted in the surface layer, with a 600 s half-life.

[19] A point $M(x, y, z, t)$ in the LES grid is assumed to belong to an updraft if it satisfies

$$q'(M) > \gamma \max(\sigma_q, \sigma_{\min}) \quad \text{and} \quad w(M) > 0 \tag{1}$$

where q' is the tracer anomaly with respect to the slab average, w is the vertical velocity at the chosen point, γ is a scale factor (chosen to be one), σ_q is the standard deviation of tracer concentration at the corresponding level, and $\sigma_{\min}$ is a minimum standard deviation designed to avoid selecting too many points in well-mixed layers. The value of $\sigma_{\min}$ proves to be especially important close to the PBL top, where turbulence is strong and updrafts detrain. The minimum standard deviation proposed by *Couvreux et al.* [2010] is

$$\sigma_{\min} = \frac{\sigma_0}{z} \int_0^z \sigma_q(k)\, \partial k \tag{2}$$

where the scaling factor σ_0 is 0.05. Tests and comparisons to LESs suggest that a value of $\sigma_0 = 0.2$ is more suited to Martian convection, as lower values yield a too large fractional coverage in the detraining zone at the PBL top. The updraft selection is considered to be satisfactory if it maximizes the heat and mass flux of the updraft for a minimum fraction coverage.

[20] We choose to apply the same kind of sampling for downdrafts, except our decaying tracer is not emitted at the

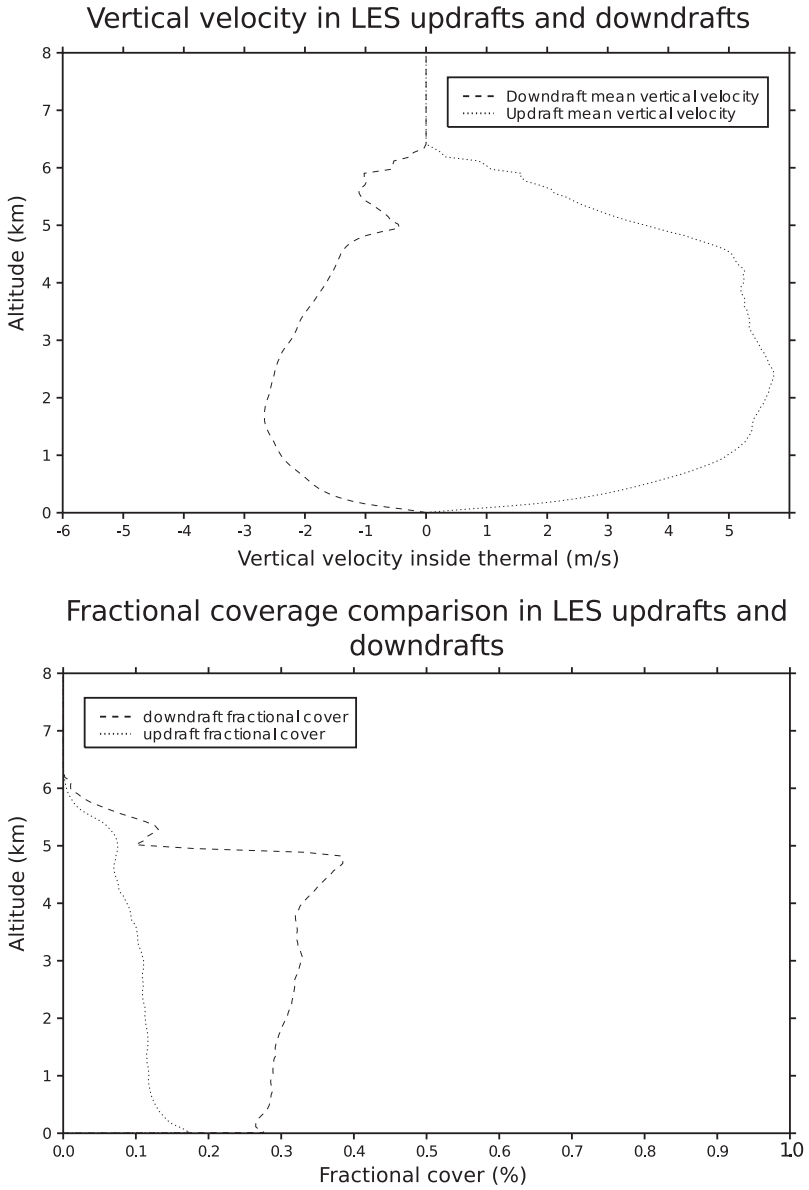

Figure 3. (top) Structure-averaged vertical velocities and (bottom) fractional coverages for updrafts (dotted lines) and downdrafts (dashed lines) using the conditional sampling technique on case I, at local time 15:00, averaged over a 925 s window.

surface but in the putative layer from which downdrafts originate. This source for downdrafts is identified in LESs as being near the PBL top (Figure 2). We compute for each time step from a first LES run the PBL height z_i, defined as the altitude at which the mean vertical velocity in the plumes reaches zero. The downdraft tracer is emitted in a second LES run at the predetermined values of z_i. To avoid cumbersome tracer repartitions in the PBL, tracer emission is only activated when the PBL height is almost stationary, between 12:00 and 17:00.

[21] A point $M(x, y, z, t)$ in the LES grid is assumed to belong to a downdraft if it satisfies

$$q'(M) > \gamma \max(\sigma_q, \sigma'_{\min}) \quad \text{and} \quad w(M) < 0 \tag{3}$$

where $\sigma'_{\min}$ is defined as in equation (2) except for integration boundaries $[z_i, z]$. To ensure that only the most prominent downward structures are sampled, the scale factor γ for tracer anomaly in equation (1) is increased from 1 to 1.5.

[22] The result of the conditional sampling criterion on both updrafts and downdrafts is illustrated in Figure 2. Structure-averaged velocities for updrafts and downdrafts are shown for case I in Figure 3, alongside fractional coverages. Downdraft velocities reach about half of the maximum updraft speed and cover a factor of 2 to 3 larger area than updrafts. In the particular example of Figure 3, downdrafts can be considered to originate between 4 and 5 km. As downward air accelerates, the plume becomes thinner. These profiles do appear like inverted updrafts starting in the inversion layer. Analyzing the downdrafts predicted in case C.large yields slightly different results than with smaller domains: fractional coverages of about 20% and vertical velocities about half of the updraft velocities.

3. A Thermal Plume Model for Mars

3.1. Two-Column Formulation

[23] Our thermal plume model for Mars is based on a modified version of the terrestrial model by *Hourdin et al.* [2002] and *Rio and Hourdin* [2008]. A thermal plume model describes a plume of air rising in the PBL through the effect of its buoyancy, fed by horizontal winds in the turbulent surface layer [*Rio and Hourdin*, 2008, Figure 1]. A model column, corresponding to a single column in GCMs' and MMs' grids, is separated into two fictive subcolumns: updraft and environment. This decomposition enables the expression of a conserved variable ϕ (potential temperature, momentum, tracer concentration, ...) separately for these two subcolumns:

$$\overline{\phi} = \alpha\,\phi_u + (1-\alpha)\,\phi_e \tag{4}$$

where α is the updraft fractional coverage and subscripts u and e, respectively, stand for updraft-averaged and environment-averaged values. Overbar quantities denote slab-averaged quantities for one model column, equivalent to slab-averaged quantities over a LES domain (the extent of which is, at best, about the grid spacing in GCMs or MMs).

[24] At each level, the thermal plume exchanges air with the environment through entrainment and detrainment. It rises while its buoyancy is positive and overshoots when its buoyancy is negative. In this process, air from lower levels rises and detrains in the environment at higher levels. This upward transport by buoyant plumes is coupled through PBL convective cells with downward compensating motions. On Earth, updrafts usually cover a small fraction of the area of a GCM or MM grid mesh: compensatory subsidences are slower and have larger fractional coverages than updrafts.

[25] Following, e.g., *Siebesma and Cuijpers* [1995], the vertical turbulent transport $\overline{w'\phi'}$ of a scalar ϕ can be formulated as

$$\begin{aligned}\overline{w'\phi'} = {} & \alpha\,\overline{w'\phi'}^{u} + (1-\alpha)\,\overline{w'\phi'}^{e} \\ & + \alpha\,(1-\alpha)\,(w_u - w_e)\,(\phi_u - \phi_e)\end{aligned} \tag{5}$$

where the prime symbol is the deviation from slab average, $\overline{w'\phi'}^{u}$ is the updraft-averaged product of deviations from the updraft average, and $\overline{w'\phi'}^{e}$ the environment-averaged product of deviations from the environment average. The first two terms in equation (5) represent the contribution of local large eddies inside the thermal plume and the environment, respectively. The third term (named organized turbulence) accounts for the transport by nonlocal large eddies, i.e., upward plumes and compensating subsidence.

[26] Terrestrial LESs have shown that the contribution to PBL transport of local eddies within thermal plumes is not significant. Hence, in Earth thermal plume models, the first term in equation (5) is neglected. In most cases, the second term is also found to be negligible and the vertical turbulent flux of ϕ simplifies to the third term. Assuming that the updraft fractional coverage α is small, α^2 terms are negligible and equation (4) yields $w_e \simeq \overline{w}$. Finally, equation (5) simplifies to

$$\overline{w'\phi'} = \frac{F_u}{\rho}(\phi_u - \phi_e) \tag{6}$$

where $F_u = \alpha\,\rho\,w_u$ is the updraft mass flux.

3.2. Three-Column Formulation With Downdrafts

[27] *Couvreux et al.* [2007] showed that the turbulent transport by downdrafts can sometimes be significant, when "dry tongues" form in the convective PBL on Earth. This questions the validity of the simplified equation (6) used in thermal plume models. This limitation appears all the more critical in the Martian convective PBL, given the intensity of downdrafts observed in LESs (Figure 1). The contribution of these downdrafts to nonlocal mixing in the daytime PBL must be taken into account.

[28] In our Martian thermal plume model, we add a downdraft subcolumn to the updraft and environment subcolumns commonly considered in terrestrial thermal plume models (see discussions in *Siebesma and Cuijpers* [1995, section 4]). This decomposition along three subcolumns is inspired by the *Tiedtke* [1989] deep convection mass flux scheme. This is in line with the fact that PBL convection, also named "shallow" convection on Earth, is actually not so shallow on Mars where nonlocal PBL transport can reach about one atmospheric scale height.

[29] The decomposition of the flux of a scalar ϕ in equation (5) now reads:

$$\begin{aligned}\overline{w'\phi'} = {} & \alpha_u\overline{w'\phi'}^{u} + \alpha_d\overline{w'\phi'}^{d} + (1-\alpha_u-\alpha_d)\overline{w'\phi'}^{e} \\ & + \alpha_u(w_u-\overline{w})(\phi_u-\overline{\phi}) + \alpha_d(w_d-\overline{w})(\phi_d-\overline{\phi}) \\ & + (1-\alpha_u-\alpha_d)(w_e-\overline{w})(\phi_e-\overline{\phi})\end{aligned} \tag{7}$$

where subscript d denotes downdraft values. The first three terms represent local turbulence within the updraft, downdraft, and environment. The last three terms are the turbulence arising from nonlocal (or organized) structures: the first one is associated with updrafts, the second one with downdrafts, and the last one with the environment. As in section 3.1, we assume local turbulence (the first two terms) can be neglected, and turbulence in the environment will be parameterized by diffusion schemes. This leads to a simplified expression for the turbulent flux of ϕ:

$$\begin{aligned}\overline{w'\phi'} = {} & \alpha_u(w_u-\overline{w})(\phi_u-\overline{\phi}) + \alpha_d(w_d-\overline{w})(\phi_d-\overline{\phi}) \\ & + (1-\alpha_u-\alpha_d)(w_e-\overline{w})(\phi_e-\overline{\phi})\end{aligned} \tag{8}$$

The turbulent kinetic energy (TKE) equation, where TKE = $0.5\,(\overline{u'^2} + \overline{v'^2} + \overline{w'^2})$ with horizontal velocities u and v, can be defined similarly (see Text S2 in the supporting information).

[30] Equation (8) can be further simplified by comparing environmental values of vertical velocity w and potential temperature θ to LESs slab-averaged values. $\theta_e = \overline{\theta}$ is a good approximation which actually holds for any conserved variable ϕ, since mixing occurs in the same way for all these variables. This yields

$$\overline{\phi} = \alpha_u\phi_u + \alpha_d\phi_d + (1-\alpha_u-\alpha_d)\phi_e \simeq \phi_e. \tag{9}$$

$\overline{w}$ corresponds to large-scale and regional vertical motions, which are both slower and less intense than PBL convective motions. To first order, we thus have in equation (8) $w_u - \overline{w} \simeq w_u$, $w_d - \overline{w} \simeq w_d$, and $w_e - \overline{w} \simeq 0$.

[31] Finally, by introducing a downward mass flux $F_d = \alpha_d\,\rho\,w_d$, the vertical turbulent transport of ϕ takes the following simple form:

$$\overline{w'\phi'} \simeq \frac{F_u}{\rho}(\phi_u - \overline{\phi}) + \frac{F_d}{\rho}(\phi_d - \overline{\phi}) \tag{10}$$

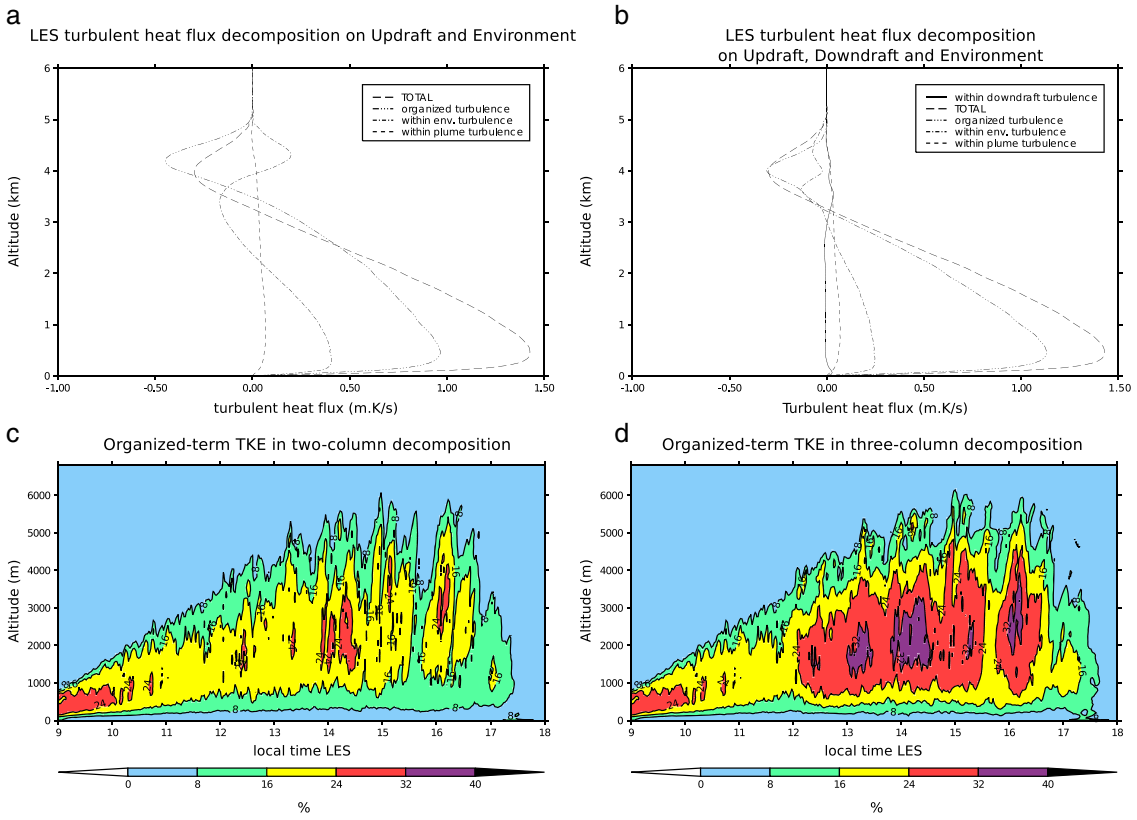

Figure 4. The role of PBL downdrafts on Mars. Decomposition of the different terms in (a) equation (5) and (b) equation (8). LES results are from case I, averaged over a 1850 s window centered on local time 13:00 and averaged over the whole domain (slab average). Long dashed lines represent the total slab-averaged value of $w'\theta'$. Slab-averaged percentage of resolved TKE associated with organized structures in the (c) terrestrial decomposition and (d) three subcolumns decomposition (results from case I). Computations before 12:00 for the latter figure are conducted assuming that downdrafts have zero fractional coverage, as the downdraft-sampling tracer is only emitted from 12:00 to 17:00. Subgrid-scale TKE from the LES diffusion scheme represents between 10 and 20% of total TKE in these cases and was added to the environmental part (because these are small eddies) for the computation of TKE percentage associated with organized structures.

This formulation completes equation (6) and distinguishes updrafts from downdrafts in a convenient way, which allows for using two-column thermal plume models developed for Earth with only minor adaptations.

3.3. Comparison of the Two Formulations

[32] To compare the two-column and three-column decompositions, we assess in LESs the partitioning of turbulent heat flux and TKE between local and nonlocal (organized) turbulent structures.

[33] For the two-column decomposition described in section 3.1, each term of the turbulent heat flux (i.e., for $\phi = \theta$ in equation (5)) is displayed in Figure 4a for one typical LES (results are similar for other cases). As is the case on Earth, local fluctuations within Martian updrafts do not contribute significantly to transport. Conversely, turbulence inside the environment contributes to almost a third of the total heat flux. This is due to both strong negative vertical velocities in downdrafts (which can reach up to two thirds of mean updraft velocities on Mars) and resolved local turbulence. Results for turbulent kinetic energy are shown in Figure 4c. According to equation (5), the contribution from nonlocal large eddies (organized turbulence) is found to represent generally between 15 and 25% (peaking locally at 35%) of the TKE resolved through LESs in the mixing layer. This would leave about 80% of TKE nonparameterized by the thermal plume model.

[34] If this remaining TKE is to be parameterized by a diffusion scheme of the *Mellor and Yamada* [1974] type, this turbulence should, ideally, only be local. This does not appear realistic on Mars. Figure 1 depicts nonlocal downward structures in the Martian PBL, correlated with broad areas of negative vertical velocities and cold temperatures. Other LES results in the literature have also shown broad downdrafts with large vertical velocities despite temperatures close to the environment along most of the vertical extension of the mixing layer [*Michaels and Rafkin*, 2004]. In the case of Mars, contrary to the Earth, these structures cannot be part of the $\overline{w'\phi'}^e$ term and considered as local turbulence. In other words, everything outside the updraft cannot be considered simply as "environmental" slowly moving air. The same remark could stand for the "dry

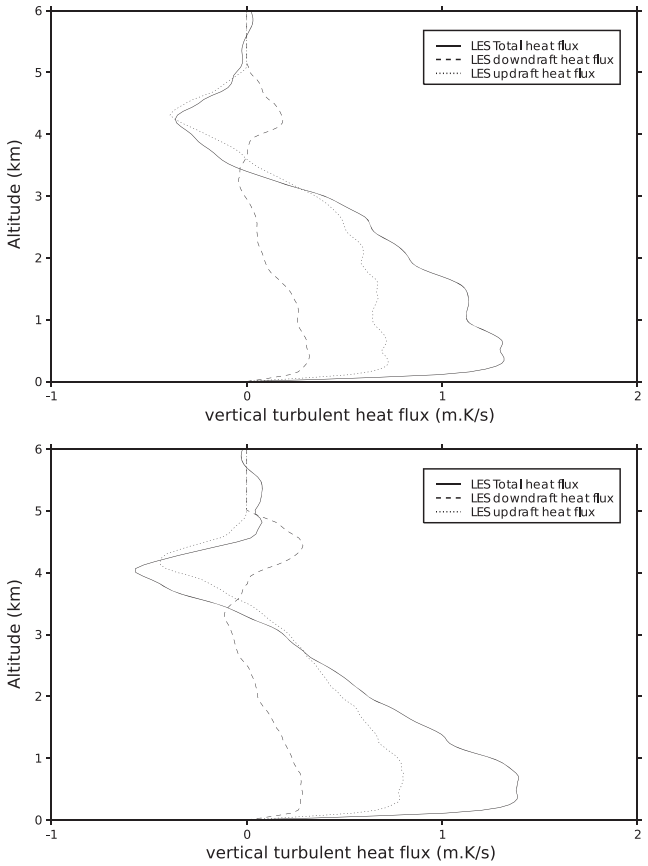

Figure 5. Contributions of downdrafts (dashed line) and updrafts (dotted line) to the total heat flux (solid line) for the LES of cases (top) A and (bottom) I at local time 13:00. Similar results are obtained for all time steps and all cases.

tongues" evidenced in the terrestrial PBL by *Couvreux et al.* [2007].

[35] What are the improvements obtained with the three-column decomposition in section 3.2? The three organized terms for heat flux ($\phi = \theta$ in equation (8)) are grouped into one and plotted in Figure 4b, alongside the three local turbulence terms. This confirms that local turbulence is negligible and that environmental turbulence can be handled by a local diffusion scheme. The organized turbulence term is found to represent 80% of the total heat flux. In our three subcolumn decomposition, the organized TKE term is generally between 25 and 40% of the total resolved TKE in LESs (Figure 4d; an analysis with case C.large yields similar conclusions). This significant increase in organized TKE, obtained by taking into account nonlocal downdrafts, confirms the conclusions in section 3.2. In the Martian atmosphere, a part of the environmental turbulence defined through terrestrial decomposition can be seen neither as a slowly compensating subsidence nor as small eddies.

4. Parameterizing Updrafts and Downdrafts

[36] The next step in developing the thermal plume model is the computation of the values of mass flux F and variables ϕ for updraft and downdraft subcolumns in equation (10).

4.1. Entrainment and Detrainment

[37] How entrainment and detrainment are parameterized is key to the thermal plume model. The vertical variation of updraft mass flux F_u (defined in section 3.1) is indeed the difference between entrainment rate ϵ and detrainment rate δ [*Rio and Hourdin*, 2008]. Hence, the steady state conservation equation for a variable ϕ at a given level in a simple updraft/environment decomposition is

$$\frac{1}{F_u}\frac{\partial F_u \phi_u}{\partial z} = \epsilon\,\phi - \delta\,\phi_u \tag{11}$$

Formulations used to extract entrainment and detrainment rates ϵ and δ from LES results are detailed in supplementary material (section 3).

[38] In equation (11), inherited from terrestrial parameterizations, thermals are assumed to be, at a given time, stationary (i.e., temporal derivative terms in equations detailed in Text S3 in the supporting information). Despite the rapid and intense growth of the Martian boundary layer during the day, profiles of ϵ and δ on Mars indicate that this simplification is still valid on Mars. A steep increase of the contribution of these terms is observed in the surface layer and corresponds to smaller-scale turbulence, represented by the source layer (a prescribed entrainment rate in the surface layer that initiates the thermal plume; the source layer is discussed in Text S4 in the supporting information). Above the inversion layer, these terms also become large, consistent with the strong plume detrainment and increase in PBL height.

4.2. Vertical Velocity Equation

[39] Many distinct formulations for ϵ and δ are described in Earth literature. In preliminary models, entrainment and detrainment rates were prescribed as being constant with height. More sophisticated parameterizations use schemes where entrainment and detrainment rates also depend on vertical velocity and buoyancy in the plume [*Rio et al.*, 2010; *de Rooy and Siebesma*, 2010].

[40] To obtain an equation for the vertical velocity, equation (11) is applied to vertical velocity w_u, with an additional term $\alpha\,\rho\,\Gamma$ that accounts for the lifting and drag forces applied to air parcels within the plume, and the continuity equation in the quasi-Boussinesq approximation is used (see Text S3 in the supporting information). With $\Omega = w_e/w_u$, this yields

$$\frac{1}{2}\frac{\partial w_u^2}{\partial z} = -\epsilon\, w_u^2\,(1-\Omega) + \Gamma \tag{12}$$

where the term $\rho\,\partial\alpha_u/\partial t$ is neglected. In terrestrial models, Ω is assumed to be 0. Nevertheless, because of the strategy we adopt to parameterize downdrafts, we set a small negative value for Ω, which slightly increases drag induced by entrainment (see section 4.4).

[41] Although realistic expressions exist for Γ [*Gregory*, 2001], this term essentially results in a positive contribution to lifting from buoyancy and a negative contribution from drag forces. Following observations on Earth, several authors proposed to reduce the drag term to a term proportional to the square of the vertical velocity [*Simpson and Wiggert*, 1969; *Bretherton et al.*, 2004]. In our Martian

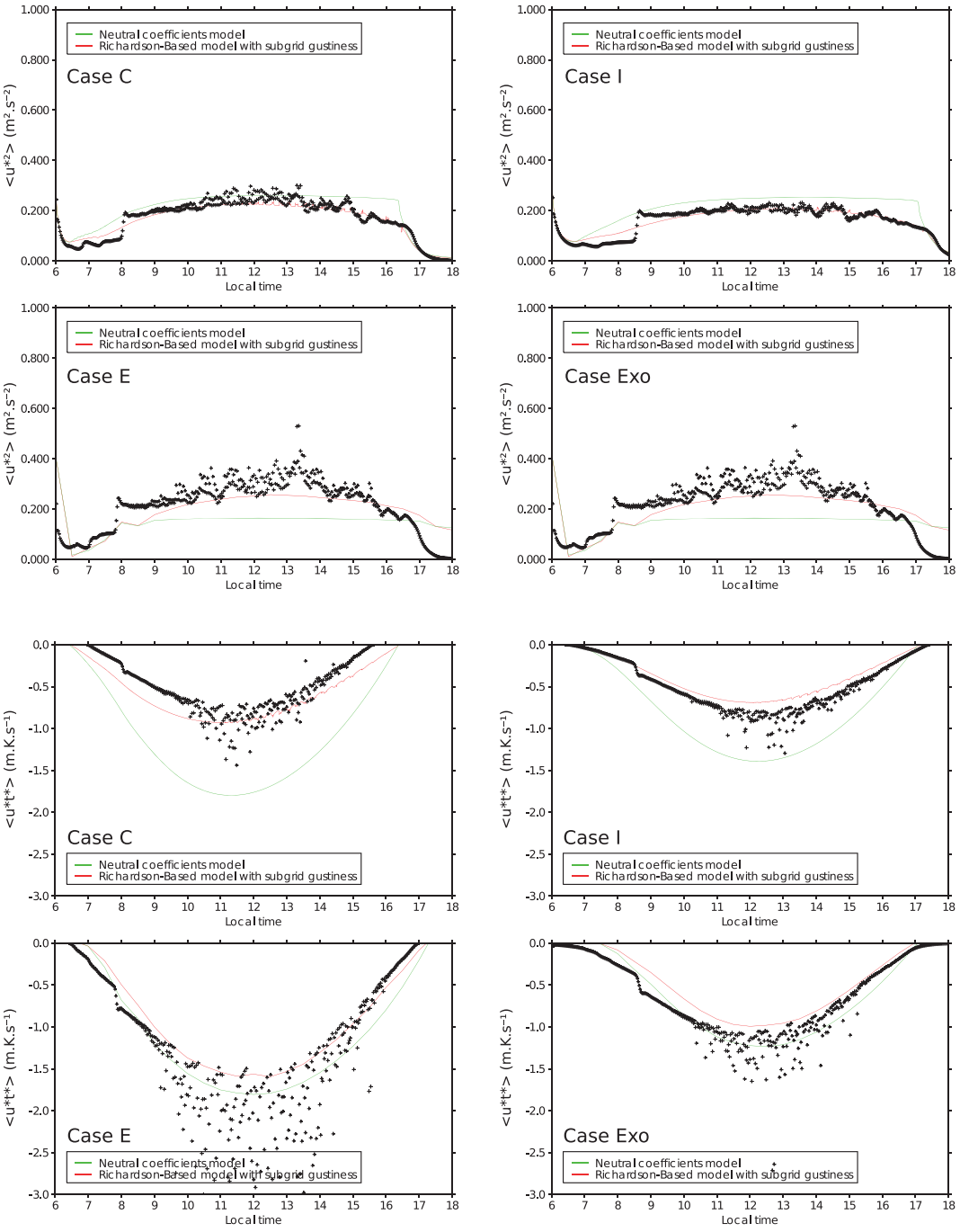

Figure 6. Comparisons of predicted $u_\star^2$ and $u_\star\theta_\star$ for cases C, I, E, and Exo between old and new surface layer models. Solid lines are SCM results and black crosses are LES results. SCM first level height is about 4.5 m, whereas LES first model level height is about 2 m.

thermal plume model, we parameterize updrafts with the approach adopted by *Rio et al.* [2010]:

$$\Gamma = a\,B - b\,w_u^2 \tag{13}$$

where B is the buoyancy and a and b are free parameters. We find that the standard setup $a = 1$ is compliant with Martian LESs which show that Γ is close to the buoyancy profile of the plume (see Figure S1 in the supporting information; we use case C.large to maximize statistical weight). These comparisons of vertical velocity profiles between the thermal plume model and LES results allow us to find the optimal value for drag term coefficient: $b = 1\times10^{-4}$. Because the vertical velocity profile also depends on ϵ, these comparisons had to be done in an iterative way. Although our parameterization slightly overestimates Γ in the upper part of the plume, it accurately describes the external forces acting on the plume throughout most of the PBL vertical extent.

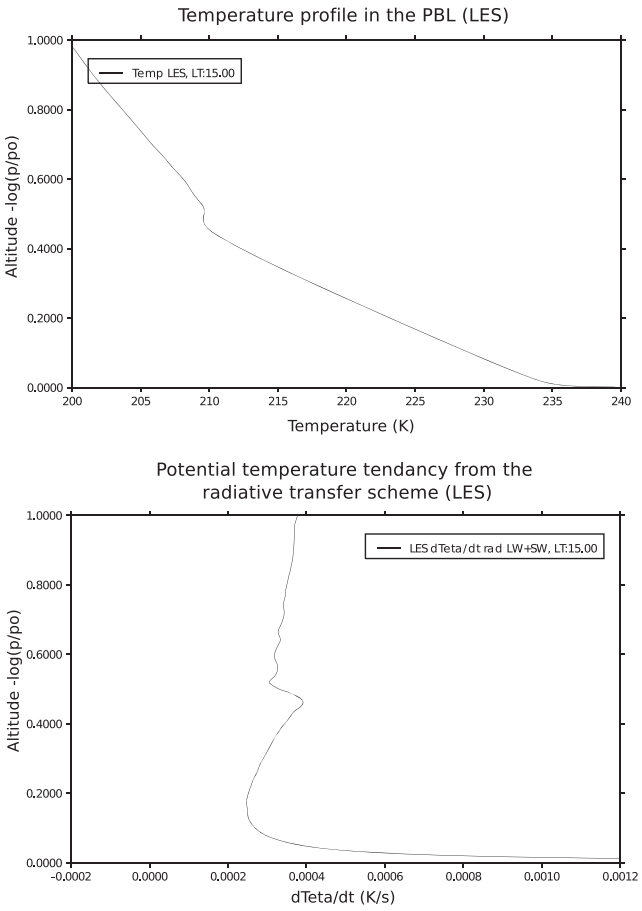

Figure 7. (top) Slab-averaged profiles of temperature and (bottom) heating rates predicted by radiative transfer at local time 15:00 for simulation case I. Heating rates include both shortwave (SW, visible wavelengths) and longwave (LW, infrared wavelengths) components. The SW contribution results mainly from direct absorption of incoming solar radiation by CO_2 and dust. In our case assuming well-mixed dust in the PBL, it is approximately constant with height. The variations with height of heating rates mostly arise from variations in LW heating rates [e.g., *Haberle et al.*, 1993].

4.3. Formulation Adopted for Entrainment and Detrainment

[42] *Nordeng* [1994] suggests that entrainment can be seen as the mechanism that compensates the reduction in fractional coverage of a nondetraining thermal due to its acceleration:

$$\epsilon = \frac{\beta_1}{w_u}\frac{\partial w_u}{\partial z} \tag{14}$$

where $\beta_1 \in [0, 1]$ is a parameter introduced by *Rio et al.* [2010] to account for real-case conditions which may depart from the ideal theoretical situation. Using equations 12 and 13, this leads to

$$\epsilon = \frac{\beta_1}{1+\beta_1}\left(a\frac{B}{w_u^2} - b\right) \tag{15}$$

This formulation was compared to our LES results for Mars. We found that ϵ tends to be underestimated in the main part of the plume (mixed layer) and overestimated in the surface layer. The alternative approach by *Gregory* [2001] (which corresponds to $b = 0$ in equation (15)) does not yield favorable results either: entrainment rate is acceptable only in the region of the plume above the surface layer.

[43] The intensity of Martian convection makes it difficult to use simple linear laws for ϵ and to reconcile distinct

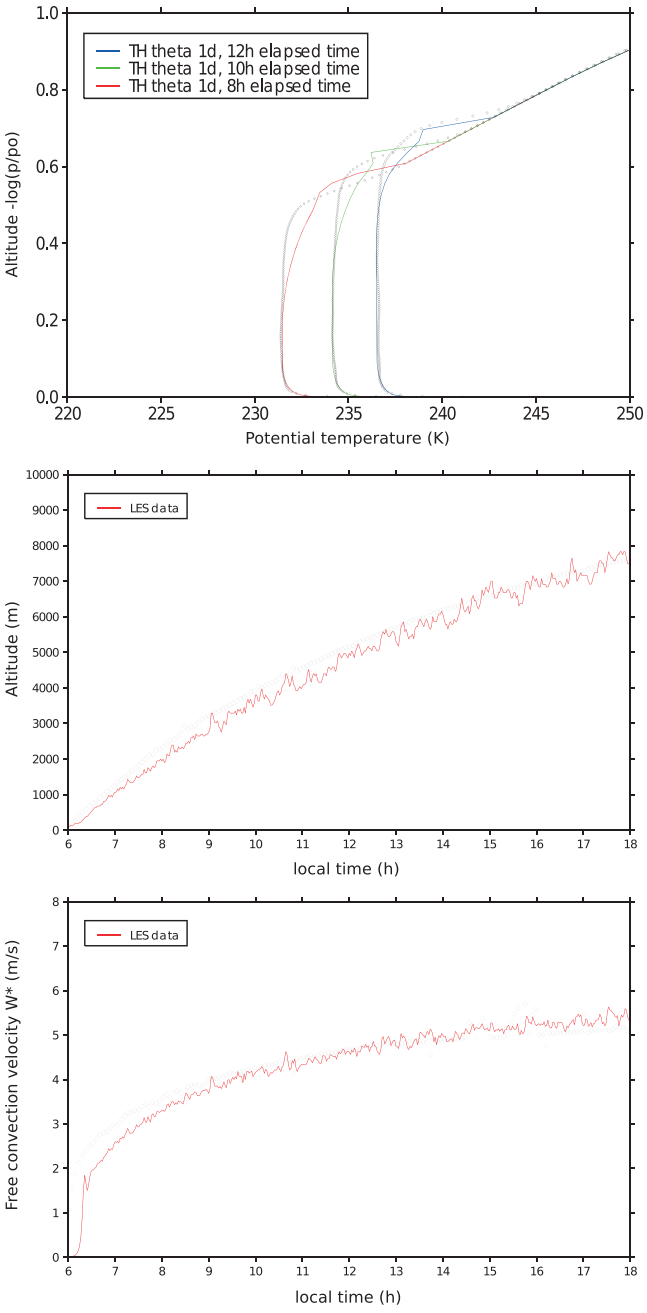

Figure 8. Comparisons between high vertical resolution SCM (solid lines) and LES (diamonds). Case with radiative transfer deactivated and sensible heat flux prescribed. Potential temperature profiles after (top) 8, 10, and 12 h of simulation, (middle) PBL height z_i, and (bottom) free convection velocity $w_\star$. Note that contributions from the local turbulence scheme are taken into account in the computation of $w_\star$, in addition to the thermal plume model contributions.

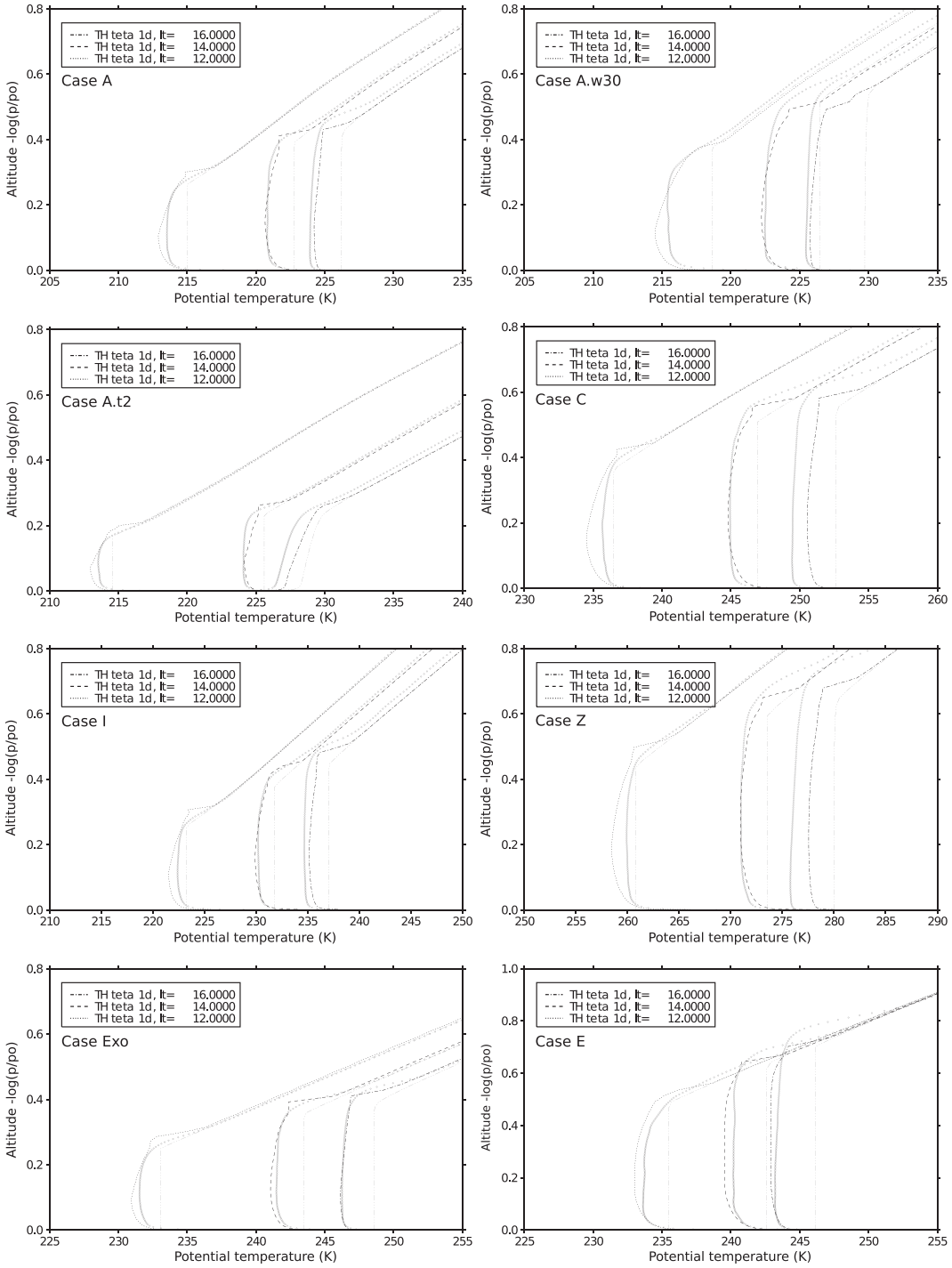

Figure 9. Potential temperature profiles from the SCM including thermals and a Richardson-based surface layer with turbulent gustiness, compared to LES results (diamonds). Results are taken at local times 12:00 (dotted lines), 14:00 (dashed lines), and 16:00 (dotted dashed lines). Results using convective adjustment scheme and old surface layer model are superimposed in triple-dotted dashed lines.

entrainment modes along the vertical extent of the plume. To address this issue, we propose to use a power-law fit between ϵ and Γ/w_u^2:

$$\epsilon = \mathcal{E}_1 \left(\frac{\Gamma}{w_u^2} \right)^{\mathcal{E}_2} = \mathcal{E}_1 \left(a \frac{B}{w_u^2} - b \right)^{\mathcal{E}_2}. \qquad (16)$$

Consistent results are obtained for all LES cases listed in Tables 1 and 2 for $\mathcal{E}_1 = 0.037$ and $\mathcal{E}_2 = 0.63$.

[44] *Rio et al.* [2010] argue that detrainment rate can be simply parameterized as proportional to $B/{w_u}^2$ above the inversion layer ($\delta = \mathcal{D}_1 B/w_u^2$ for $B < 0$) and constant below it ($\delta = \mathcal{D}_2$ for $B \geq 0$). Detrainment rate parameterizations have

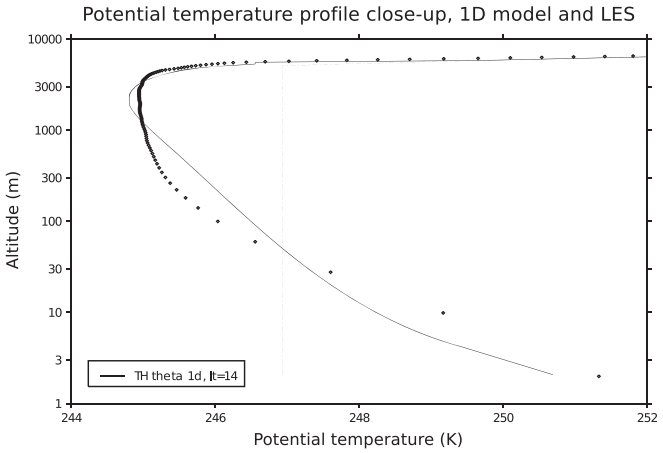

Figure 10. Potential temperature profile for case C at local time 14:00, plotted against a logarithmic altitude axis. LES results are shown as diamonds, SCM using the thermal plume model as a solid line, and SCM with convective adjustment as a dotted dashed line.

proven to be difficult to fit to detrainment computed directly from LESs. Acceptable results (though with less precision than for entrainment rates) can however be obtained by performing fits to spatially and temporally averaged LES results, which yields the values $\mathcal{D}_1 = -0.67$ and $\mathcal{D}_2 = 4 \times 10^{-4}$.

[45] Nondimensional entrainment, detrainment, and mass flux are used to discretize equation (11) along the vertical. Details on the mathematical formulation of the model and its discretization are included in the supporting information (Text S4). A normalization flux F_c must be used to get the entrainment and detrainment mass fluxes E and D from ϵ and δ. We follow *Hourdin et al.* [2002] who proposed to compute F_c using the horizontal/vertical aspect ratio r of PBL convective cells (cf. Text S4 in the supporting information). Martian LESs predict aspect ratios ranging from 1 to 3 depending on local time and chosen scenario. Dry terrestrial LES studies also show variations of the aspect ratio, with values ranging from 1 to 5. Given this variability, and the fact that aspect ratios on Mars are difficult to infer from existing measurements, we choose to keep the aspect ratio r as a free parameter. Adjusting r mainly changes the potential temperature profile in the surface layer for a given mass flux. Therefore, r can be set by using potential temperature profiles from LESs. For a wide range of realistic conditions, we found that $r = 1$ gives satisfying results, while any value below 0.7 yields insufficient mixing.

4.4. Treatment of Downdrafts

[46] The downdraft term in equation (10) is analogous to the updraft term and hence can be modeled with a similar approach. The equivalent of equation (11) for a downdraft is

$$\frac{1}{F_d}\frac{\partial F_d \phi_d}{\partial z} = \epsilon_d \phi - \delta_d \phi_d \tag{17}$$

where F_d is the downdraft mass flux and ϕ_d is the value of ϕ in the downdraft.

[47] In the parameterization for the updraft subcolumn, the estimated buoyancy of the plume is used to compute a vertical velocity profile for an air parcel, accounting for drag forces. Relating downdrafts to pure buoyant motions is not as straightforward as for updrafts. Downdrafts with positive buoyancy in their initiation part are often found in Martian LESs. This is also a common problem for Earth models [*Couvreux et al.*, 2005]. Because of these uncertainties on underlying mechanisms, parameterizations based on vertical velocity are not considered as relevant for now. Instead, we choose to use a simpler parameterization for downdrafts.

[48] We found in LESs that the downdraft-to-updraft ratio of mass flux F_d/F_u is constant with height in the mixing layer (see Figure S2 in the supporting information). This ratio is ~ -0.8, an absolute value less than 1, as could be expected from the behavior of a typical thermal plume whose compensating flux is downward. Furthermore, this value is, to first order, similar for all local times and all simulated cases. Hence, we obtain F_d from F_u with a proportionality law in the mixed layer and a decreasing linear law in the surface layer:

$$F_d = -\zeta F_u \quad \text{with} \quad \zeta = \max\left(0.8\,,\, 4\,\frac{z}{z_i} + 0.6\right) \tag{18}$$

Since $F_d < F_u$, this parameterization induces a slow compensating subsidence in the environment, meaning that $w_e \neq 0$ hence $\Omega < 0$. Considering fractional coverages for downdrafts in Figure 3, we estimate Ω to be about –3%. This correction is negligible given the rough setting of the drag parameter b to calculate Γ: Reasonable results are also obtained with $\Omega = 0$.

[49] To complete the prescription of downdraft heat fluxes, we simply set a potential temperature profile for downdrafts from environment properties:

$$\theta_d = \xi\, \theta_e \quad \text{with} \quad \xi = \min\left(1\,,\, \frac{1}{400}\frac{z}{z_i} + 0.9978\right) \tag{19}$$

where coefficients are chosen so that parameterized turbulent heat fluxes (diurnal cycle and vertical profile) are satisfyingly reproduced in the surface layer and mixed layer compared to LES results in Figure 5. Good results are also obtained in the inversion layer provided that a fine enough vertical grid is adopted to resolve overshoots (see section 6).

[50] Prescribing downdraft quantities allows us to compute temperature tendencies through downdraft heat flux

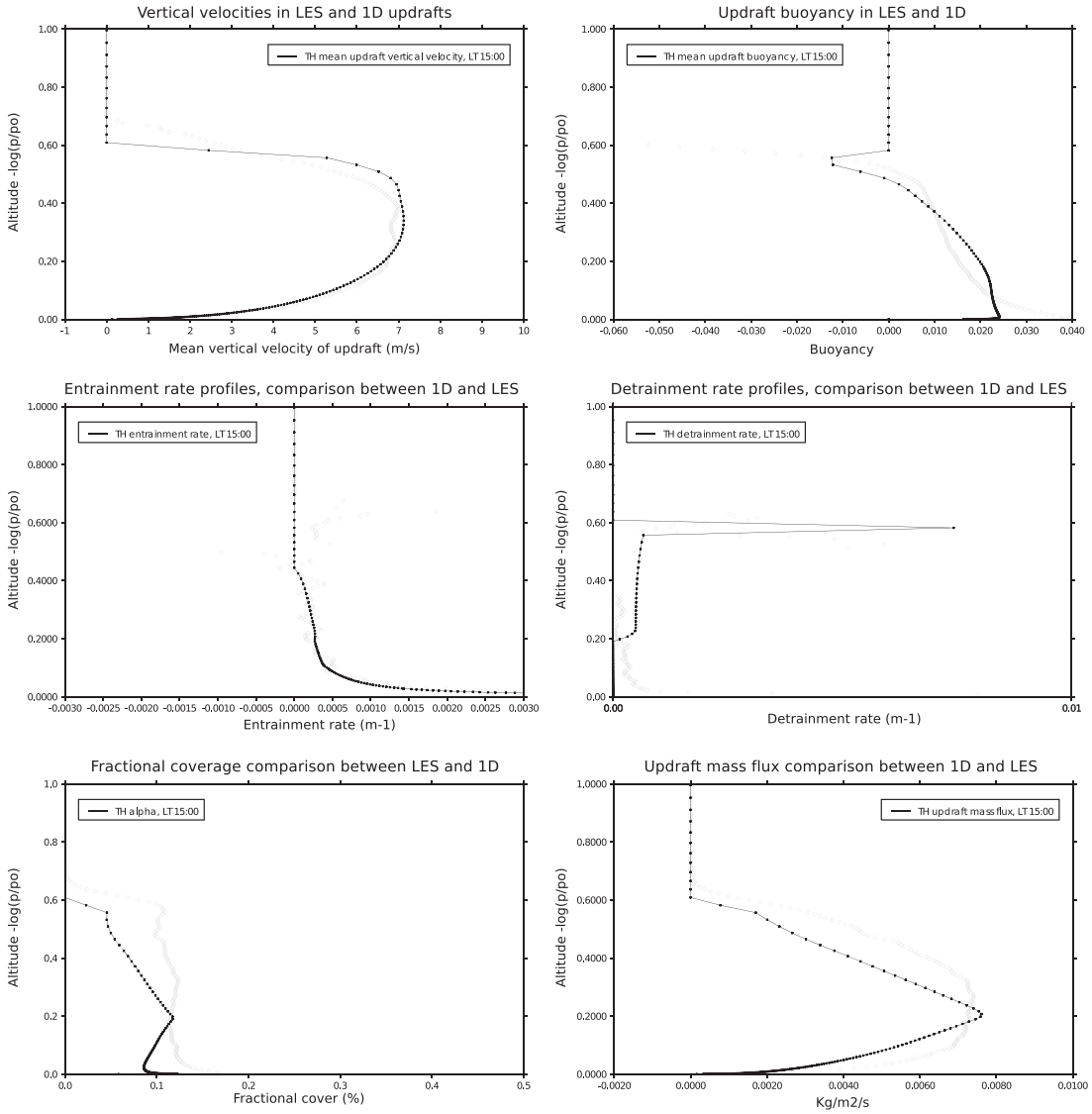

Figure 11. Intermediate variables of the thermal plume model for case C at local time 15:00. From top to bottom, left to right: vertical velocity, updraft buoyancy, entrainment rate, detrainment rate, fraction coverage, updraft mass flux. In all plots, LES results are shown as diamonds and SCM results as solid lines with bullets.

divergence. Because entrainment and detrainment rates are unknown, it is not possible to deduce tracer and momentum transport in the downdraft, unless one computes entrainment and detrainment rates from prescribed mass flux and prescribed potential temperature profiles. The latter approach has proven to be difficult for downdrafts. As a result, for now in the thermal plume model, only downward transport of tracer and momentum related to compensatory subsidence in the environment is taken into account. Future work is needed to overcome this limitation.

5. Surface Layer Parameterization

[51] Since surface-atmosphere fluxes control the amount of heat and momentum leaving the surface, and being transported and mixed by PBL eddies, parameterizations for PBL mixing must be coupled to a surface layer scheme to compute surface-atmosphere interactions. Here we present a surface layer parameterization based on a Monin-Obukhov Richardson formulation and coupled to turbulent gustiness estimated from our Martian thermal plume model. This improved surface layer scheme is important to predict more accurately the near-surface atmospheric state measured by Mars landers (see section 6.4).

[52] The principle of surface layer schemes is that momentum and heat fluxes between surface and atmosphere, denoted $u_\star^2$ and $u_\star\theta_\star$, respectively, are computed by multiplying the difference between surface and atmospheric values with aerodynamic conductances: $\Lambda_m = C_D U_0$ for momentum and $\Lambda_h = C_H U_0$ for heat (where U_0 is the norm of the horizontal wind at the model first layer at altitude z_1 and C_D and C_H are momentum and heat bulk transfer coefficients). One of the simplest parameterizations for surface-atmosphere momentum and heat fluxes is the neutral coefficient formulation, where $C_D = C_{DN} = (\kappa/\ln(z_1/z_0))^2$

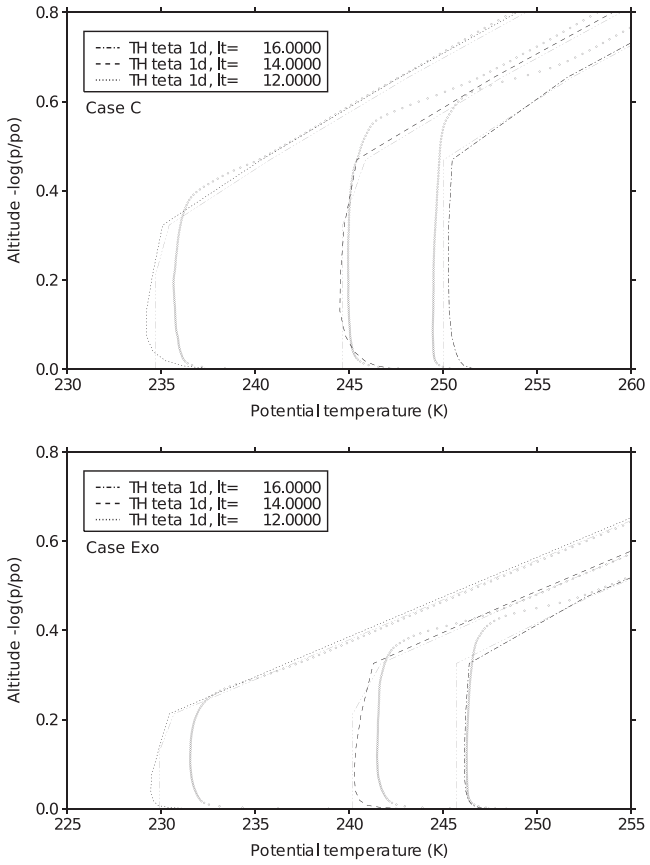

Figure 12. Temperature profiles from the SCM using the Mars LMD GCM vertical and temporal resolution, including the thermal plume model and a Richardson-based surface layer at different local times (dotted, dashed, and dotted dashed lines), compared to LES results (diamonds). Results using the convective adjustment scheme and neutral coefficients surface layer model are superimposed in triple-dotted dashed lines.

and $C_H = C_{DN}$ (κ is Von Karman's constant and z_0 the roughness length). This simple parameterization tends to overestimate exchange fluxes and does not take into account atmospheric stability in the computation of transfer coefficients, which is especially problematic on Mars where near-surface stability is highly variable on the diurnal scale.

[53] Using a Monin-Obukhov similarity theory to compute transfer coefficients on Mars yields more realistic results than a neutral bulk scheme [*Haberle et al.*, 1993; *Tillman et al.*, 1994; *Sävijarvi*, 1999; *Martínez et al.*, 2009]. Text S5 in the supporting information details the formulation of our Monin-Obukhov surface layer scheme, the computation of the bulk Richardson number R_i, and our choice for the stability coefficients and functions f_m,f_h. In this model, transfer coefficients for heat and momentum C_D and C_H are $C_D = f_m(R_i)\, C_{DN}$ and $C_H = f_h(R_i)\, C_{HN}$.

[54] We can use our new thermal model to further improve this surface layer scheme, especially as far as the coupling between surface and mixed layers is concerned. Indeed, LESs show that turbulent horizontal motions associated with nonlocal turbulence contribute to surface-atmosphere exchange fluxes; yet surface layer schemes are used in GCMs and MMs where this gustiness is left unresolved. To remedy to this, we follow an idea described by *Redelsperger et al.* [2000] who argue that the wind U_0 in aerodynamic conductances Λ_m and Λ_h should be replaced by a modified wind U combining the large-scale (synoptic) wind U_0 near the surface with a gustiness wind U_g:

$$U^2 = U_0^2 + U_g^2 \tag{20}$$

U_0 is also what we named background wind in LESs (section 2). U_g reflects the intensity of PBL convective winds and can be computed following different methods. For instance, *Godfrey and Beljaars* [1991] propose to define $U_g = \beta w_\star$, where $w_\star$ is the free convection velocity and β a constant parameter. The main advantage of linking U_g and $w_\star$ in a GCM or MM parameterization is that the latter quantity can be extracted from the thermal plume model.

[55] Is this linear relationship between U_g and $w_\star$ valid for Mars? One of the limitations is that $w_\star$ has to be redefined for Mars given the strong radiative forcing in the daytime PBL (see *Spiga et al.* [2010, equation 12], for the definition of $w_\star$ for Martian applications). Taking advantage of the large number of points available in LES results, we can build a good statistical estimate of gustiness wind $U_g = \sqrt{U^2 - U_0^2}$. Resulting statistics of gustiness speeds at each time step can then be compared to $w_\star$. We find that U_g is not perfectly linear with $w_\star$ (see Figure S3 in the supporting information) owing to a threshold effect for high values of vertical velocity scale. Interestingly, this is also noted in *Redelsperger et al*. [2000] with a different proxy for convective activity. We therefore use a fit to a logarithmic law defined as follows:

$$U_g = \log(1 + 0.7\, w_\star + 2.3\, w_\star^2) \tag{21}$$

This approach takes into account large-eddy gustiness for most cases, which ensures that coupling the thermal plume and surface layer models yields similar surface-atmosphere exchange fluxes to LESs. However, the above function is not optimal in conditions of large background winds (30 m/s in the mixed layer). Proxies of the convective activity other than $w_\star$ do not solve this issue. Those difficulties to model gustiness at large background wind speeds have also been noted by *Fenton and Michaels* [2010] and deserve dedicated studies.

[56] Comparisons between parameterized values and LESs results for $u_\star^2$ and $u_\star \theta_\star$ are shown in Figure 6. Results comparing the neutral and new R_i-based surface layer models are shown. Changes in the description of $u_\star^2$ are minor yet reflect gustiness-enhanced fluxes. Changes in $u_\star \theta_\star$ are important and highlight how the neutral model severely overestimates C_H.

6. Performance of the New Martian PBL Schemes

[57] Here we assess the performance of single-column Martian simulations using our Martian thermal plume model and Richardson-based surface layer with turbulent gustiness. The thermal plume model only accounts for nonlocal turbulent transport. A Mellor and Yamada 2.5 diffusion scheme is employed for small-scale mixing and local mixing by large eddies [see *Hourdin et al.*, 2002, Appendix B]. Other physical parameterizations (namely, radiative transfer) are otherwise similar to Martian LES carried out in this study

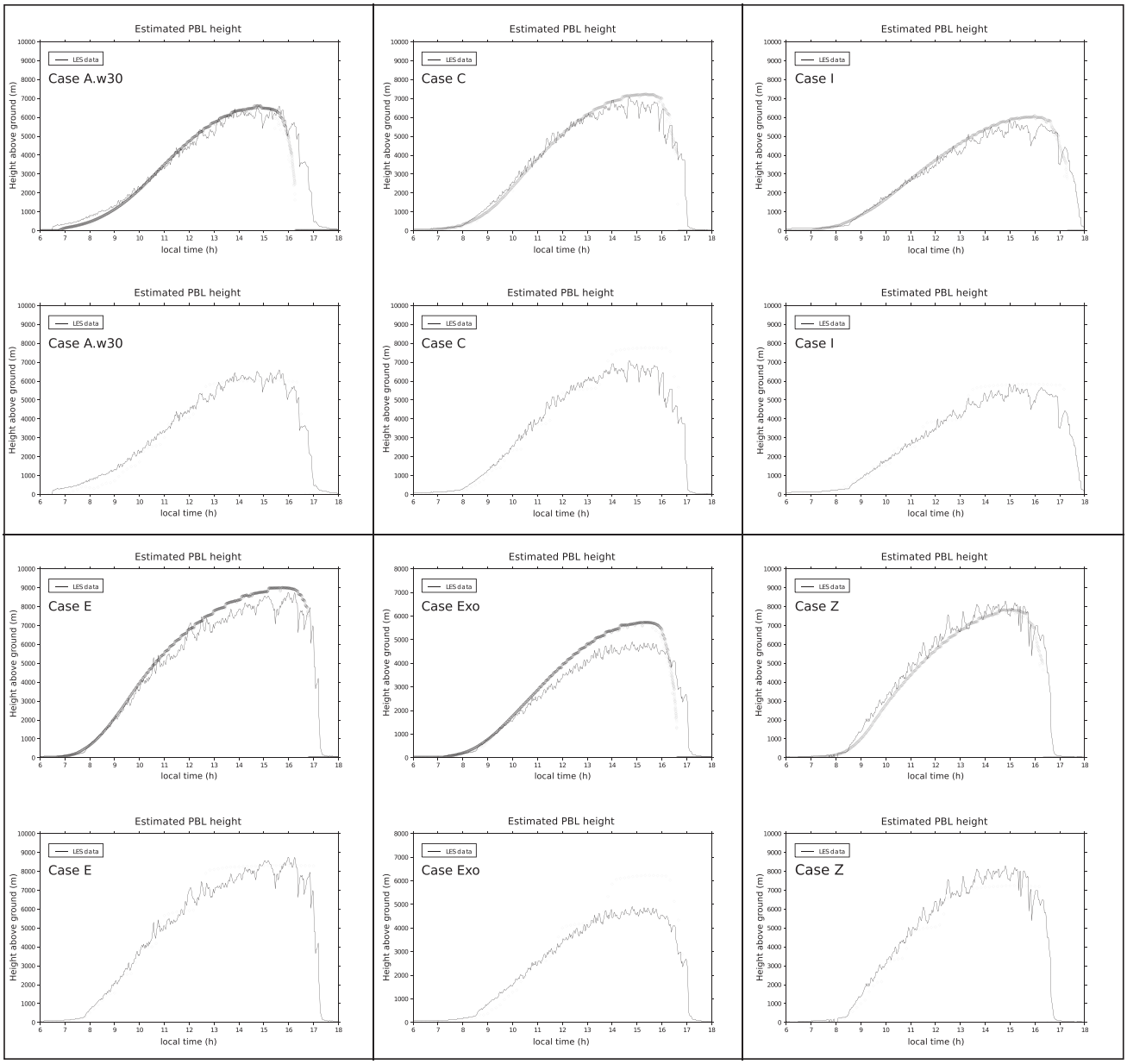

Figure 13. Comparisons of maximum height reached in the thermals between LES (solid line) and SCM (diamonds). Vertical scales can be different between figures. For a given case, top figures are obtained using high resolution and bottom figures are the corresponding GCM-like resolution results.

(see section 2). Subsurface layers are initialized with a 2 year "warmup" run in our SCM. Model predictions are eventually validated against lander measurements in the near-surface of Mars.

6.1. SCM Without Radiation

[58] Single-column simulations are first run at similar vertical resolution and integration time step as LESs. This aims at assessing the performance of our new parameterizations alone, without any bias arising from unresolved gradients in coarse vertical discretizations. An additional specific setting is needed to pursue this aim. Figure 7 shows that in the PBL, radiation and convection are closely intertwined. Notably, the PBL top exhibits a local temperature enhancement which corresponds to the overshoot region for thermal plumes where their remaining advected heat is deposited: this causes radiative cooling at the PBL top and warming above and below.

[59] The validity of the Martian thermal plume model, and surface layer, is first assessed without radiative transfer, in a case which resembles dry PBL convection on Earth. A fixed sensible heat flux is prescribed in LES and SCM to $\overline{w'\theta'}_0$ = 1.5 K m/s to reproduce typical PBL dynamics obtained in case C. Potential temperature profiles in both SCM and LES are compared in Figure 8 (top). Temperature inversion in the surface layer is well represented by the thermal plume model compared to the LES. The overshoot region near PBL top is also reproduced, although with less precision. Because this

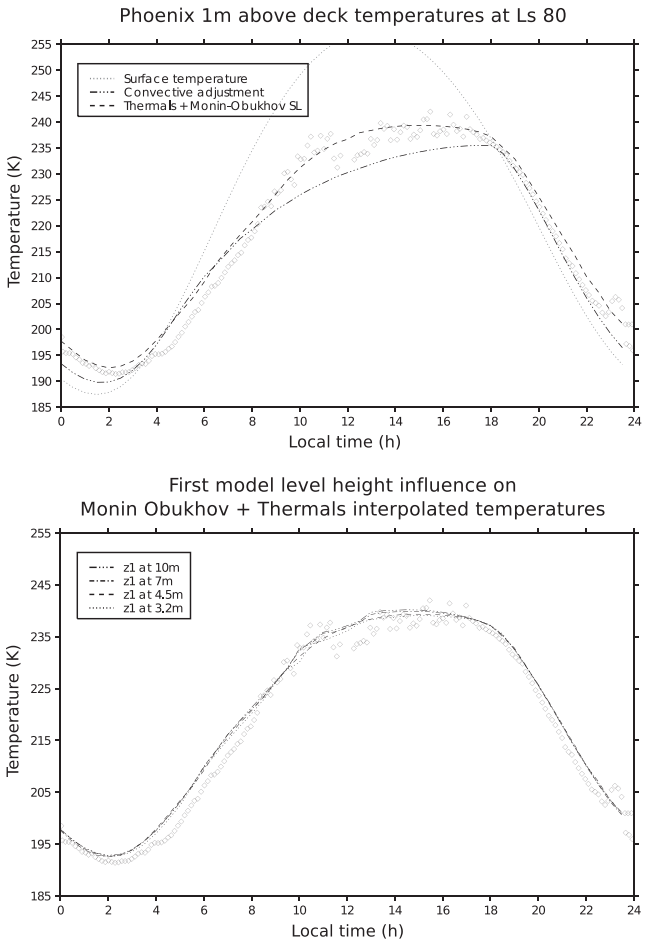

Figure 14. (top) Phoenix measured temperatures at 1 m above deck and SCM results. Phoenix data are plotted in diamonds and results from the SCM with lines. Convective adjustment temperature at 1 m (dotted dashed line) is obtained by running the SCM with convective adjustment using a first model level at 2 m (rover deck itself is at 1 m above ground). Results using the thermals and improved surface layer (dashed line) are obtained by running the SCM with a first model level at 4.5 m and running a Monin-Obukhov interpolation at 2 m. (bottom) Phoenix measured temperatures at 1 m above deck and Monin-Obukhov interpolation with varying first model level height z_1 between 3.2 and 10 m. Phoenix data are plotted in black diamonds and results from the SCM in black lines (see legend for linestyles). (Since convective adjustment predicts sharp temperature transitions between surface and atmosphere, a Monin-Obukhov interpolation is not possible with this PBL scheme. Because the idea behind convective adjustment is to produce a neutral potential temperature gradient in the PBL, we run our SCM including convective adjustment with a first model level at 2 m and take the temperature value at this level for the comparison with data).

detraining layer is much more dynamic in LESs, it is inherently more challenging to parameterize precisely. However, we note that PBL top is accurately reproduced in potential temperature profiles. Mixed layer temperatures predicted by the SCM are in agreement with LESs along most of the PBL depth, despite values slightly too low in the overshoot region. PBL height in the SCM is estimated using the predicted vertical velocity profile and compared to the height at which the vertical velocity in plumes cancels out in the LES (Figure 8; all diagnostics are domain averaged in LES). Although a slight offset is present, PBL height is correctly predicted by the SCM, meaning that the overshoot region of thermals is adequately parameterized. Finally, we compare free convection velocity $w_\star$ (calculated from maximum vertical eddy heat flux and PBL height according to equation 12 in *Spiga et al.* [2010]) between LES and SCM in Figure 8 [middle and bottom]. Predictions from the SCM in Figure 8 are found to be satisfyingly close to LES results.

6.2. SCM With Radiation

[60] We now explore all the realistic Martian cases described in Tables 1 and 2. A refined vertical grid is used as in section 6.1. Results from the SCM are compared to LESs in Figure 9, along with results obtained with dry convective adjustment. Our thermal plume model for Mars ensures that temperatures in the mixing layer are satisfyingly close to those predicted by LESs. The new scheme is especially efficient in maintaining a superadiabatic layer near the Martian surface (Figure 10), which is a key characteristic of the daytime PBL in this environment [*Smith et al.*, 2006]. This will ensure in Mars GCMs, MMs, and SCMs that surface-atmosphere exchange fluxes and near-surface temperature profiles will be correctly estimated (especially in very convectively active cases). The prediction of the inversion layer is also satisfactory, as well as the reproduction of daytime growth of PBL height. Late afternoon temperatures in the SCM tend to be too warm, not only in the PBL but also in the troposphere. However, in this part of the convective PBL, SCM results are closer to LES case C.large than LES case C. These LESs differ by a slightly lower model top and a much larger domain extension. About 30 thermal plumes are found at a given time in case C.large, hence improving the statistics. Furthermore, convective cells are less constrained by the boundary conditions and can be represented in their full horizontal extent. Velocity scales $w_\star$ in the SCM are in agreement with LES results (see Figure S4 in the supporting information), which indicates that PBL convective activity is well reproduced by a SCM using our Martian thermal plume model.

[61] Key "intermediate" variables in the thermal plume model are the vertical velocity and buoyancy which determine entrainment and detrainment rates. In turn, those variables being coupled, it is difficult to get correct buoyancy and vertical velocity without correct entrainment and detrainment rates. Fractional coverages and total mass fluxes are also key diagnostics to check the robustness of our thermal plume model. Figure 11 shows that those parameterized intermediate variables in the thermal plume model compare well with predicted variables in LES integrations. This demonstrates that our thermal plume model is capable of parameterizing the nonlocal transport through PBL convective structures in a physically consistent way. While being overall satisfyingly accounted for by our thermal plume model, mass flux (and, consequently, fractional coverage) profiles tend to exhibit a peaking shape, which reflects the assumptions made on the source profile in the surface layer (see Text S4.1 in the supporting information).

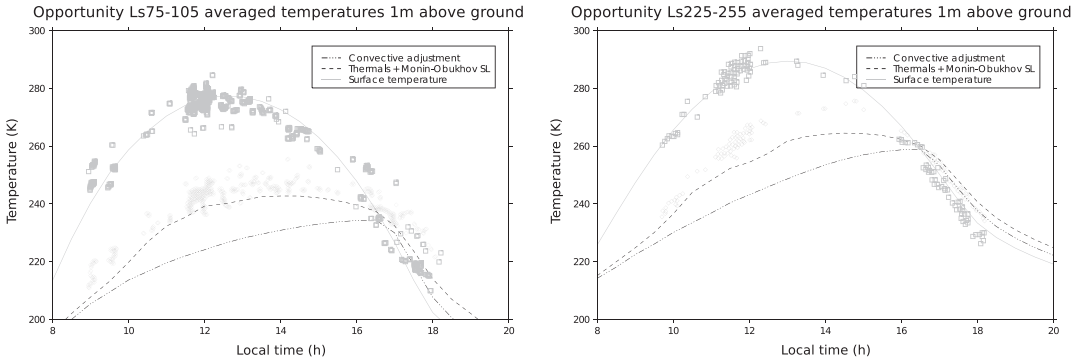

Figure 15. Opportunity measured temperatures at 1 m above ground and surface temperatures averaged between L_s = 75° and L_s = 105° (left) and between L_s = 225° and L_s = 255° (right), from downward-looking mini-TES. Rover data for surface temperature are shown as gray squares and temperatures at 1 m as black diamonds. SCM results are shown as lines. Convective adjustment temperature at 1 m is obtained by running the SCM with convective adjustment using a first model level at 1 m (triple-dotted black line). Results using the thermals and improved surface layer are obtained by running the SCM with a first model level at 4.5 m and running a Monin-Obukhov interpolation at 1 m (dashed line). SCM surface temperature is similar for both configurations and is shown with a plain gray line. Data are from *Smith et al.* [2006].

An alternate formulation for this source term, perhaps more suitable for the radiatively controlled lower Martian PBL, would be needed to improve these diagnostics in the thermal plume model.

6.3. SCM With Radiation and Coarse Vertical Grid ("GCM-Like")

[62] To work most adequately, the thermal plume model should use a vertical grid with fine enough resolution to resolve gradients of intermediate quantities in the model (e.g., buoyancy profiles), especially in the superadiabatic region above the surface and the overshoot region in the vicinity of the PBL top. It is difficult to achieve such vertical resolution in Mars GCMs which often use about one level for each kilometer in the PBL (and refined resolution near the surface). We thus test the thermal plume model with a SCM adopting typical GCM vertical grids (e.g., for Mars LMD GCM, 33 levels up to 130 km) and physical time steps (four per Martian hour). The vertical levels within the PBL in this configuration are set approximately to (2 m, 15 m, 60 m, 160 m, 360 m, 0.7 km, 1.2 km, 2 km, 3.2 km, 4.7 km, 6.6 km, 8.9 km, 11.6 km) above the surface. Some adaptations are needed for our local diffusion scheme to yield reliable results (see Text S6 in the supporting information). We evaluate the accuracy of the thermal plume model for PBL temperature profiles in Figure 12, PBL height in Figure 13, convective velocity scale $w_\star$, and vertical eddy heat flux (Figures S4 and S5, respectively, in the supporting information). Although slightly less accurate than the results obtained with a finer vertical grid in section 6.2 (especially in the overshoot region near the PBL top), the thermal plume model used on a coarse, "GCM-like," vertical grid enables reliable estimates of PBL-related quantities resolved in LESs. The superadiabatic layer near the Martian surface is well reproduced by the thermal plume model compared to LES results. The good agreement shown in Figure 13 between the SCM and LES predictions of PBL height is also a particularly satisfying point. LES predictions of PBL height for most cases in Table 1 are supported by radio-occultation measurements [*Hinson et al.*, 2008; *Spiga et al.*, 2010]. Furthermore, PBL height using our Martian thermal plume model are consistent with LES predictions, contrary to existing PBL parameterizations for Mars which tend to underestimate PBL height compared to LES [*Tyler et al.*, 2008].

6.4. Comparisons With Lander Measurements

[63] To further validate our Martian thermal plume model and surface layer scheme, we compare predictions using our new schemes with lander measurements on Mars (data from Phoenix lander and Opportunity rover).

[64] Data at L_s = 80° from the temperature sensor of the Phoenix polar lander [*Davy et al.*, 2010] are compared with results from our SCM. Surface pressure is extracted from the MCD (p_s = 848 Pa), surface roughness from *Hébrard et al.* [2012] (z_0 = 0.27 cm), and dust opacity from Thermal Emission Spectrometer (TES) observations (τ = 0.18). Albedo is also extracted from TES measurements $\mathcal{A}$ = 0.24; a value of thermal inertia $\mathcal{T}$ = 165 tiu is used instead of the TES value of nighttime apparent thermal inertia ($\mathcal{T}$ = 250 tiu) to better reflect observed nighttime temperatures (and the overall shape of the diurnal cycle). A constant background wind of 20 m s^{-1} is prescribed in the free atmosphere. Figure 14 (top) shows a comparison between the 2 m temperature sensor, and SCM results, consistently interpolated using Monin-Obukhov similarity theory from the first model level at 4.5 m above ground to 2 m above ground. Predictions with our new PBL schemes are satisfyingly close to measurements, especially compared to the use of convective adjustment which underestimates afternoon temperature by at least 5 K. Figure 14 (bottom) shows the results obtained through varying the height of the first layer in the SCM from 3 to 10 m. Parametrization is robust to changes in vertical discretization, meaning that fluxes and gradients are correctly represented.

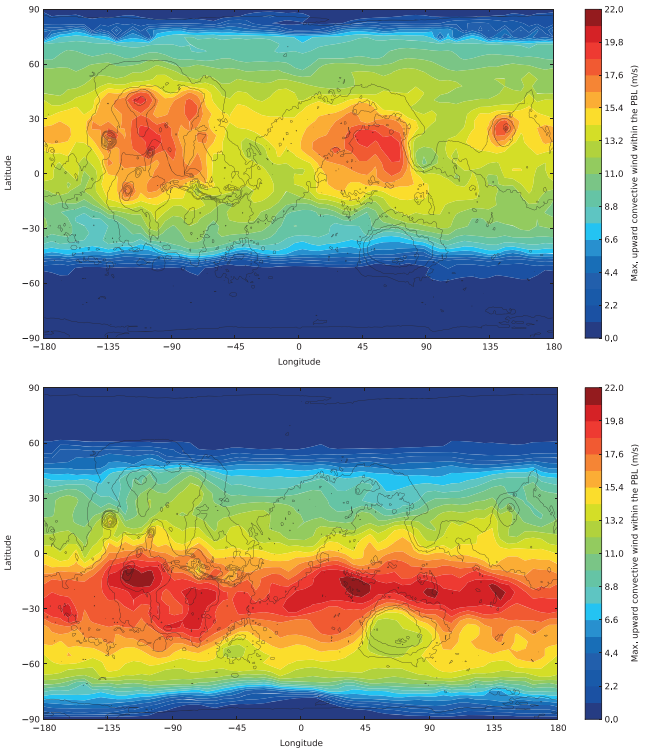

Figure 16. Longitude-latitude map of the estimated maximum velocities inside updrafts in the convective PBL at northern summer and winter solstices, obtained from the thermal plume model included in the Mars LMD GCM [*Forget et al.*, 1999; *Madeleine et al.*, 2011]. Results for all grid points are shown at local time 13:00.

[65] We then choose two series of data acquired by mini-TES 1 m above ground [*Smith et al.*, 2006] on board the Opportunity rover close to the Martian equator: one in northern summer (L_s = 75-105°) and one in northern winter (L_s = 225-255°). SCM settings are defined from similar sources as for Phoenix (z_0 = 0.92 cm, p_s = 634 Pa and τ = 0.27 in summer, p_s = 679 Pa and τ = 0.72 in winter). Thermal inertia $\mathcal{T}$ = 120 tiu and albedo $\mathcal{A}$ = 0.14 for summer, and $\{\mathcal{A} = 0.23; \mathcal{T} = 290$ tiu$\}$ for winter, are obtained by fitting the predicted diurnal cycle of surface temperature with measurements (TES values are $\mathcal{T}$ = 280 tiu and $\mathcal{A}$ = 0.18). Distinct locations for the rover at the two considered seasons is a likely explanation for this difference in ground properties. Figure 15 shows results for the two seasons. Results using the thermal plume model and Monin-Obukhov surface layer are in agreement with the data. Predicted values are too cold by a few kelvins, but results with our new model offer a significant improvement compared to the use of convective adjustment which leads to a severe underestimation (as much as 15 K) of daytime near-surface temperatures.

[66] Interestingly, model predictions appear closer to observations in northern summer at low dust loading than in northern winter when the atmosphere is dustier. More measurements are clearly needed to address this question. However, a possible cause is that the Monin-Obukhov approach is less valid when dust opacity is higher. The validity of the Monin-Obukhov similarity theory on Mars is actually still left to be confirmed. The problem stems from the assumption of constant vertical heat flux made on the explicit form of the generic stability functions ϕ_m and ϕ_h (see supporting information). This assumption might be flawed on Mars where radiative forcing near the surface is strong, especially when dust loading in the atmosphere is large. The Monin-Obukhov limitations in situations of strong radiative forcing require theoretical studies which are left as future work.

6.5. An Example of Use in a GCM

[67] We included our thermal plume model, and surface layer parameterization, in a version of the LMD GCM [*Forget et al.*, 1999] with recent improvements of the radiative transfer [*Madeleine et al.*, 2011]. The vertical discretization is the one described in section 6.3. We use four physical time steps per Martian hour instead of two in the version of *Forget et al.* [1999]. This time step refinement yields more accurate results from the thermal plume model (compared to LES), especially as far as the coupling between radiation and convection is concerned, while being also beneficial to other parameterizations (e.g., cloud formation).

[68] Contrary to existing PBL parameterizations for the Martian atmosphere, our new thermal plume model enables us to estimate to first order, and map, key PBL variables such as convective velocity scale $w_\star$ and maximum vertical eddy heat flux $\langle w'\theta' \rangle_{\max}$. Given those two variables, profiles of vertical eddy heat flux and vertical velocity variance can then be reconstructed from the Martian similarity relationships in *Spiga et al.* [2010]. In addition to this, the maximum intensity $w_{\max}$ of vertical winds inside daytime PBL updrafts and downdrafts can be estimated by

$$w^u_{\max} \sim 2.75\, w_\star \qquad w^d_{\max} \sim 1.75\, w_\star \tag{22}$$

GCM maps for $w^u_{\max}$ are given in Figure 16. The convective activity is maximum either in low-albedo (Syrtis Major) or high-topography (Tharsis, Elysium, southern high-cratered terrains) areas, while it is diminished within giant impact craters (Hellas, Argyre). This is in agreement with radio-occultation measurements [*Hinson et al.*, 2008] and LESs [*Spiga et al.*, 2010]. Another possible use of $w_\star$ is to use equation (21) to map near-surface horizontal gustiness due to PBL convection.

7. Conclusion

[69] We propose an adaptation of the terrestrial plume model of *Hourdin et al.* [2002] and *Rio and Hourdin* [2008] to the intense Martian PBL convection. Modifications are needed in the Martian case, because in this low-density, radiatively controlled environment, what is named "shallow" convection on Earth is actually not so shallow. We show that downdrafts contribute significantly to the transport in the PBL, as they represent nonlocal turbulence that cannot be handled by a local diffusion scheme (e.g., Mellor and Yamada scheme). Our reformulated parameterization of thermals is inspired by terrestrial deep convection schemes using three-parcel decompositions for each grid point: an updraft, a downdraft, and an environment. In addition to our new thermal plume model for Mars, we propose an improved surface layer model. Our new surface layer is based on Monin-Obukhov similarity theory, uses a Richardson

formulation for stability functions, and accounts for the contribution of turbulent gustiness in surface-atmosphere fluxes. With the new thermal plume model and surface layer parameterization, the near-surface atmospheric structure predicted by climate models is much closer to the one predicted by turbulence-resolving LESs. Furthermore, GCMs and MMs are then able to compute more accurate predictions for key turbulent quantities, such as free convection velocity scale, PBL height, and maximum vertical turbulent heat flux. This permits extensive mapping of such quantities, or reconstructions of turbulent profiles, without having to run LESs. The code of our Martian thermal plume model is available upon request to the authors.

[70] Characterizing daytime convective plumes through LESs makes our parameterization prone to the same limitations as the LES approach. Martian LESs performed thus far use periodic boundary conditions, and assume flat topography, uniform surface properties (albedo, thermal inertia), and dust loading in the domain. While the general principles of the thermal plume model presented in this paper remain valid, its "fine tuning" could be affected by those limitations. For instance, a small-scale crater, or contrasts of albedo, might alter how frequent and strong updrafts would be. Sampling these structures will yield different constraints for the thermal plume model. Hence, we expect our scheme to be refined as LESs improve in the future and as more measurements are available to validate them.

[71] Our new PBL parameterizations have broad implications for Martian atmospheric studies. Improvements obtained for the PBL wind and temperature structures are likely to impact the predictions of GCMs and MMs and possibly the understanding of Martian atmospheric dynamics. Moreover, how dust particles, major climatic agents on Mars, are lifted from the surface, injected in the first meters of the atmosphere, and then transported above the PBL remains an open question in which the knowledge of PBL processes is a key factor of progress. Finally, our work will hopefully allow for better estimation of atmospheric hazards met by landing spacecraft which will explore Mars in the future. Our approach for PBL parameterizations is also an extreme example which can be of interest for terrestrial meteorology.

[72] **Acknowledgments.** We warmly thank the three reviewers whose thorough comments helped to improve and clarify the paper. We acknowledge support from CNES and ESA.

References

Balme, M. R., and R. Greeley (2006), Dust devils on Earth and Mars, *Rev. Geophys.*, *44*, RG3003, doi:10.1029/2005RG000188.

Bretherton, C., J. McCaa, and H. Grenier (2004), A new parameterization for shallow cumulus convection and its application to marine subtropical cloud-topped boundary layers. Part I: Description and 1D results, *J. Atmos. Sci.*, *132*, 883–896.

Couvreux, F., F. Guichard, J. L. Redelsperger, C. Kiemle, V. Masson, J. P. Lafore, and C. Flamant (2005), Water-vapour variability within a convective boundary-layer assessed by large-eddy simulations and IHOP_2002 observations, *Q. J. R. Meteorol. Soc.*, *131*, 2665–2693, doi:10.1256/qj.04.167.

Couvreux, F., F. Guichard, V. Masson, and J.-L. Redelsperger (2007), Negative water vapour skewness and dry tongues in the convective boundary layer: Observations and large-eddy simulation budget analysis, *Boundary Layer Meteorol.*, *123*(2), 269–294.

Couvreux, F., F. Hourdin, and C. Rio (2010), Resolved versus parametrized boundary-layer plumes. Part I: A parametrization-oriented conditional sampling in large-eddy simulations., *Boundary-Layer Meteorol.*, *134*, 441–458, doi:10.1007/s10546-009-9456-5.

Davy, R., J. A. Davis, P. A. Taylor, C. F. Lange, W. Weng, J. Whiteway, and H. P Gunnlaugson (2010), Initial analysis of air temperature and related data from the Phoenix MET station and their use in estimating turbulent heat fluxes, *J. Geophys. Res.*, *115*, E00E13, doi:10.1029/2009JE003444.

de Rooy, W., and A. Siebesma (2010), Analytical expressions for entrainment and detrainment in cumulus convection, *Q. J. R. Meteorolog. Soc.*, *136*, 1216–1227, doi:10.1002/qj.640.

Fenton, L., and T. I. Michaels (2010), Characterizing the sensitivity of daytime turbulent activity on Mars with the MRAMS LES: Early results, *Int. J. Mars Sci. Explor.*, *5*, 159–171, doi:10.1555/mars.2010.0007.

Forget, F., F. Hourdin, R. Fournier, C. Hourdin, O. Talagrand, M. Collins, S. R. Lewis, P. L. Read, and J.-P. Huot (1999), Improved general circulation models of the Martian atmosphere from the surface to above 80 km, *J. Geophys. Res.*, *104*, 24,155–24,176.

Godfrey, J. S., and A. C. M. Beljaars (1991), On the turbulent fluxes of buoyancy, heat and moisture at the air-sea interface at low wind speeds, *J. Geophys. Res.*, *96*, 22,043–22,048.

Gregory, D. (2001), Estimation of entrainment rate in simple models of convective clouds, *Q. J. R. Meteorolog. Soc.*, *127*, 53–72.

Haberle, R., H. C. Houben, R. Hertenstein, and T. Herdtle (1993), A boundary layer model for Mars: Comparison with Viking lander and entry data, *J. Atmos. Sci.*, *50*, 1544–1559.

Hébrard, E., C. Listowski, P. Coll, B. Marticorena, G. Bergametti, A. Määttänen, F. Montmessin, and F. Forget (2012), An aerodynamic roughness length map derived from extended Martian rock abundance data, *J. Geophys. Res.*, *117*, E04008, doi:10.1029/2011JE003942.

Hinson, D. P., M. Pätzold, S. Tellmann, B. Häusler, and G. L. Tyler (2008), The depth of the convective boundary layer on Mars, *Icarus*, *198*, 57–66, doi:10.1016/j.icarus.2008.07.003.

Hourdin, F., F. Couvreux, and L. Menut (2002), Parameterization of the dry convective boundary layer based on a mass flux representation of thermals, *J. Atmos. Sci.*, *59*, 1105–1123, doi:10.1175/1520-0469(2002)059.

Hourdin, F., et al. (2012), Lmdz5b: The atmospheric component of the IPSL climate model with revisited parameterizations for clouds and convection, *Clim. Dyn.*, *79*, 2193–2222, doi:10.1007/s00382-012-1343-y.

Lilly, D. K. (1962), On the numerical simulation of buoyant convection, *Tellus*, *14*(2), 148–172.

Madeleine, J.-B., F. Forget, E. Millour, L. Montabone, and M. J. Wolff (2011), Revisiting the radiative impact of dust on Mars using the LMD global climate model, *J. Geophys. Res.*, *116*, E11010, doi:10.1029/2011JE003855.

Malin, M. C., and K. S. Edgett (2001), Mars global surveyor mars orbiter camera: Interplanetary cruise through primary mission, *J. Geophys. Res.*, *106*, 23,429–23,570, doi:10.1029/2000JE001455.

Martínez, G., F. Valero, and L. Vázquez (2009), Characterization of the martian convective boundary layer, *J. Atmos. Sci.*, *66*, 2044–2058.

Mellor, G. L., and T. Yamada (1974), A hierarchy of turbulence closure models for planetary boundary layers, *J. Atmos. Sci.*, *31*, 1791–1806.

Mellor, G. L., and T. Yamada (1982), Development of a turbulence closure model for geophysical fluid problems, *Rev. Geophys.*, *20*(4), 851–875.

Michaels, T. I., and S. C. R. Rafkin (2004), Large eddy simulation of atmospheric convection on Mars, *Q. J. R. Meteorol. Soc.*, *130*, 1251–1274, doi:10.1256/qj.02.169.

Millour, E., et al. (2008), The latest (version 4.3) Mars climate database, in *Mars Atmosphere Modelling and Observations*, edited by F. Forget, p. 9029, LPI Contribution No. 1447, Williamsburg, Virginia.

Moeng, C., J. Dudhia, J. Klemp, and P. Sullivan (2007), Examining two-way grid nesting for large eddy simulation of the PBL using the WRF model, *Mon. Weather Rev.*, *135*(6), 2295–2311.

Nordeng, T., (1994), Extended versions of the convective parameterization scheme at ECMWF and their impact on the mean and transient activity of the model in the tropics, *ECMWF Tech. Memo. 206,* 41 pp, Shinfield Park, Reading RG2 9AX, United Kingdom.

Rafkin, S. C. R. (2003), The effect of convective adjustment on the global circulation of Mars as simulated by a general circulation model, in *Sixth International Conference on Mars*, July 20–25 2003, abstract no. 3059, edited by A. Albee, Pasadena, Calif.

Redelsperger, J., F. Guichard, and S. Mondon (2000), A parameterization of mesoscale enhancement of surface fluxes for large-scale models, *J. Climate*, *13*, 402–421.

Richardson, M. I., A. D. Toigo, and C. E. Newman (2007), PlanetWRF: A general purpose, local to global numerical model for planetary

atmospheric and climate dynamics, *J. Geophys. Res.*, *112*, E09001, doi:10.1029/2006JE002825.

Rio, C., and F. Hourdin (2008), A thermal plume model for the convective boundary layer: Representation of cumulus clouds, *J. Atmos. Sci.*, *65*, 407–425, doi:10.1175/2007JAS2256.1.

Rio, C., F. Hourdin, F. Couvreux, and A. Jam (2010), Resolved versus parametrized boundary-layer plumes. Part II: Continuous formulations of mixing rates for mass-flux schemes, *J. Atmos. Sci.*, *134*, 441–458, doi:10.1007/s10546-010-9478-z.

Sävijarvi, H. (1999), A model study of the atmospheric boundary layer in the Mars Pathfinder lander conditions, *Q. J. Roy. Meteor. Soc.*, *125*(554), 483–493.

Savijärvi, H., and T. Siili (1993), The Martian slope wind and the nocturnal PBL jet, *J. Atmos. Sci.*, *50*, 77–88.

Schofield, J. T., D. Crisp, J. R. Barnes, R. M. Haberle, J. A. Magalhaães, J. R. Murphy, A. Seiff, S. Larsen, and G. Wilson (1997), The Mars Pathfinder Atmospheric Structure Investigation/Meteorology (ASI/MET) experiment, *Science*, *278*, 1752–1757.

Siebesma, A. P., and J. W. M. Cuijpers (1995), Evaluation of parametric assumptions for shallow cumulus convection, *J. Atmos. Sci.*, *52*, 650–666, doi:10.1175/1520-0469(1995)052.

Simpson, J., and V. Wiggert (1969), Models of precipitating cumulus towers, *Mon. Weather Rev.*, *97*, 471–489., doi:10.1175/1520-0493(1969)097.

Skamarock, W. C., and J. B. Klemp (2008), A time-split nonhydrostatic atmospheric model for weather research and forecasting applications, *J. Comput. Phys.*, *227*, 3465–3485, doi:10.1016/j.jcp.2007.01.037.

Smith, M. D., M. J. Wolff, N. Spanovich, A. Ghosh, D. Banfield, P. R. Christensen, G. A. Landis, and S. W. Squyres (2006), One Martian year of atmospheric observations using MER Mini-TES, *J. Geophys. Res.*, *111*, E12S13, doi:10.1029/2006JE002770.

Soares, P., P. Miranda, A. Siebesma, and J. Teixeira (2004), An eddy-diffusivity/mass-flux parametrization for dry and shallow cumulus convection, *Q. J. Roy. Meteor. Soc.*, *130*(604), 3365–3383.

Spiga, A. (2011), Elements of comparison between Martian and terrestrial mesoscale meteorological phenomena: Katabatic winds and boundary layer convection, *Planet. Space Sci.*, *59*, 915–922, doi:10.1016/j.pss.2010.04.025.

Spiga, A., and F. Forget (2009), A new model to simulate the Martian mesoscale and microscale atmospheric circulation: Validation and first results, *J. Geophys. Res.*, *114*, E02009, doi:10.1029/2008JE003242.

Spiga, A., F. Forget, S. R. Lewis, and D. P. Hinson (2010), Structure and dynamics of the convective boundary layer on Mars as inferred from large-eddy simulations and remote-sensing measurements, *Q. J. Roy. Meteorol. Soc.*, *136*, 414–428, doi:10.1002/qj.563.

Teixeira, J., et al. (2011), Tropical and sub-tropical cloud transitions in weather and climate prediction models: The GCSS/WGNE pacific cross-section intercomparison (GPCI), *B. Am. Meteorol. Soc.*, *24*, 5223–5256.

Tiedtke, M. (1989), A comprehensive mass flux scheme for cumulus parameterization in large-scale models, *Mon. Wea. Rev.*, *117*, 1179–1800.

Tillman, J. E., L. Landberg, and S. E. Larsen (1994), The boundary layer of Mars: Fluxes stability, turbulent spectra and growth of the mixed layer, *J. Atmos. Sci.*, *51*(12), 1709–1727.

Toigo, A. D., and M. I. Richardson (2003), Meteorology of proposed Mars Exploration Rover landing sites, *J. Geophys. Res.*, *108*(E12), 8092, doi:10.1029/2003JE002064.

Troen, I., and L. Mahrt (1986), A simple model of the atmospheric boundary layer: Sensitivity to surface evaporation, *Boundary-layer Meteorol.*, *37*, 129–148.

Tyler, D., J. R. Barnes, and R. M. Haberle (2002), Simulation of surface meteorology at the Pathfinder and VL1 sites using a Mars mesoscale model, *J. Geophys. Res.*, *107*(E4), 5018, doi:10.1029/2001JE001618.

Tyler, D., J. R. Barnes, and E. D. Skyllingstad (2008), Mesoscale and large-eddy simulation model studies of the Martian atmosphere in support of Phoenix, *J. Geophys. Res.*, *113*, E00A12, doi:10.1029/2007JE003012.